Title
On Fundamental Issues Of Vehicle Steering Control For Highway

Authors
Guldner, Jurgen
Tan, Han-shue

Publication Date
1997

CALIFORNIA PATH PROGRAM
INSTITUTE OF TRANSPORTATION STUDIES
UNIVERSITY OF CALIFORNIA, BERKELEY

On Fundamental Issues of Vehicle Steering Control for Highway Automation

Jürgen Guldner
Han-Shue Tan
Satyajit Patwardhan

California PATH Working Paper
UCB-ITS-PWP-97-11

This work was performed as part of the California PATH Program of the University of California, in cooperation with the State of California Business, Transportation, and Housing Agency, Department of Transportation; and the United States Department Transportation, Federal Highway Administration.

March 1997

ISSN 1055-1417

On Fundamental Issues of Vehicle Steering Control for Highway Automation

*Jürgen Guldner, Han-Shue Tan and Satyajit Patwardhan**

California PATH
University of California at Berkeley
Institute of Transportation Studies
1357 S. 46th Street, Richmond, CA 94804-4698

Abstract

Automatic steering control for passenger cars, a vital control subsystem of Automated Highway systems (AHS), has been studied for several decades. Different reference systems have been examined for detecting the lateral vehicle displacement from the lane center, employing a variety of modern control methods to design automatic steering controllers. Implementations of the AHS relevant subclass of 'look-down' reference systems, however, have encountered practical constraints and limitations, especically for highway speed driving. By analyzing the lateral vehicle dynamics in the light of these practical constraints and limitations, we establish a general framework for automatic steering control in an AHS environment and contrast various directions for control design.

*List of authors was chosenrandomly

Keywords: Automated highway systems, automatic steering control, lane keeping control, lateral vehicle control

1 Introduction

Automatic steering control is a vital component of highway automation, currently investigated worldwide in several programs, e.g. ITS in the US (see e.g. [1]) and ASV, SSVS and ARTS under ITS Japan [2, 3]. Highway automation is a main subject of research and development of Advanced Vehicle Control Systems (AVCS). AVCS refers to the subclass of Intelligent Transportation Systems (ITS) aimed at increasing safety and throughput of road traffic while decreasing environmental impacts. Overviews of highway automation were given, for example, by Bender [4], a review of AVCS was presented by Shladover [5], and a possible AHS scenario was outlined by Varaiya [6].

For individual vehicles within an Automated Highway System (AHS), two control tasks arise. The first task, longitudinal control, involves controlling the vehicle speed to maintain a proper spacing between vehicles. This paper concentrates on the second task, lateral control, which is concerned with automatic steering of vehicles for lane keeping to follow a reference along the lane center.

Automatic steering control approaches can be grouped into *look-ahead* and *look-down* systems, according to the point of measurement of the vehicle lateral displacement from the lane reference. Look-ahead systems replicate human driving behavior by measuring the lateral displacement *ahead* of the vehicle. The look-ahead distance usually is increased with increasing velocity, similar to human behavior. A number of research groups have sucessfully conducted highway speed experiments with look-ahead systems like machine vision. Examples are VaMoRs-P [7], VITA-I and II [8, 9], and related projects (e.g. [10]) within the European PROMETHEUS Program, Carnegie Mellon University's PANS [11], and California PATH's stereo-vision based system [12]. In an effort to remedy the susceptibility of machine vision to variation of light and weather conditions, radar reflective stripes with look-ahead capability have been developed and tested at The Ohio State University (OSU) [13]. Alternatively, look-ahead laser radar systems [14] and "energy emitting or reflecting" road reference systems [15] have been studied.

Look-down reference systems, on the other hand, measure the lateral displacement at a location within or in the close vicinity of the vehicle boundaries, typically straight *down* from the front bumper. Examples are electric wire guidelines first tested at OSU [16] in the US for passenger cars and later by Daimler-Benz and MAN in Germany for city buses [17], radar reflecting guard rails studied at OSU [18], and magnetic markers used in the California PATH project [19, 20] and, most recently, in Japan [2]. Comprehensive overviews were given e.g. by Shladover [5] and Fenton [21]. However, despite an impressive amount of literature on theoretical control designs (not listed here), no highway speed experiments have been reported to the best of the author's knowledge. Furthermore, most of the practical requirements like accuracy, comfort, and robustness could not be met simultanously in most experimentally verified approaches. Notable exceptions are the experiments performed at OSU in the 70's [16], achieving up to 35 m/s (126 km/h, approx. 80 mph) under idealized

conditions and with a look-down sensor located at more than 1 m in front of an already very long vehicle, effectively resulting in a look-ahead system.

Despite the low speed limitation in experiments with true look-down reference systems to low speed, it was generally assumed possible to transfer the low speed results to highway speeds by appropriate tuning of the controllers. Unfortunately, this may not be an easy task due to significant changes in the vehicle dynamics for increasing speed. We have shown in [22] that the extension of look-down systems to practical conditions of an AHS environment with speeds above 30 m/s (108 km/h, approx. 67.5 mph) is nontrivial and requires complete rethinking of the approach. The goal of this paper is to study the fundamentals of automatic steering control for highway driving in a general framework based on physical insight. Rather than directly persuing a numeric control design, an in-depth analysis of the system and of the design requirements is first presented. This analysis is shown to lead to a distinct basis for control design. Various design directions are examined, stressing their interrelations and discussing respective practical implementation issues.

Section 2 describes the system model and control design requirements. The plant and the controller to be designed are analyzed in Section 3 using various tools of dynamic system analysis. Section 4 is devoted to a study of main design directions based on the insight gained from the system analysis.

2 Problem Description

In this section, we present a description of the automatic steering control problem. Emphazising on physical interpretation rather than on complexity and accuracy of details, linearized models are used throughout this study. The design requirements concentrate on practical and implementational issues based on the AHS experience gained at California PATH for almost a decade [20, 23].

2.1 Model for automatic steering control

A linearized model has proved sufficient for studying car steering under 'normal' conditions, i.e. non-emergency situations [24]. Assuming small angles, this allows to use the classical single-track model of Riekert-Schunk [25] shown in Fig. 1, also referred to as the "bicycle model". The two front wheels and the two rear wheels are respectively lumped together into a single wheel at the front and rear axles, and the center of gravity (CG) is located in the plane of the road surface. A linear tire model is used under the assumption of small angles during normal highway driving conditions within the physical limits of tires. The model variables denote:

$\mathbf{v}$	vehicle velocity vector with $v = \|\mathbf{v}\| > 0$; speed v is assumed measurable,
β	side slip angle between vehicle longitudinal axis and velocity vector $\mathbf{v}$ at CG,
Ψ	vehicle yaw angle with respect to a fixed inertial coordinate system,
$\ddot{y}_{CG}$	lateral acceleration at CG,
$\ddot{y}_S$	lateral acceleration at sensor S, and
δ_f	front wheel steering angle.

The linearized 2D model with two interal states, side slip angle β and yaw rate $\dot{\Psi}$, and front wheel steering angle δ_f as an input can be found e.g. in [24, 26] as

$$\frac{\mathrm{d}}{\mathrm{d}t}\begin{bmatrix} \beta \\ \dot{\Psi} \end{bmatrix} = \begin{bmatrix} -\dfrac{\mu(c_f + c_r)}{Mv} & -1 + \dfrac{\mu(c_r\ell_r - c_f\ell_f)}{Mv^2} \\ \dfrac{\mu(c_r\ell_r - c_f\ell_f)}{I_\Psi} & -\dfrac{\mu(c_f\ell_f^2 + c_r\ell_r^2)}{I_\Psi v} \end{bmatrix} \begin{bmatrix} \beta \\ \dot{\Psi} \end{bmatrix} + \begin{bmatrix} \dfrac{\mu c_f}{Mv} \\ \dfrac{\mu c_f \ell_f}{I_\Psi} \end{bmatrix} \delta_f, \qquad (1)$$

with parameters defined as:

M	total vehicle mass,
I_ψ	total vehicle inertia about vertical axis at CG,
$\ell_f(\ell_r)$	distance of front(rear) axle from CG with $\ell = \ell_f + \ell_r$,
d_S	"look-ahead" distance between sensor location S and CG,
$c_f(c_r)$	front(rear) tire cornering stiffness,
μ	road adhesion as a factor of effective tire cornering stiffness $c_f^* = \mu c_f$ $(c_r^* = \mu c_r)$.

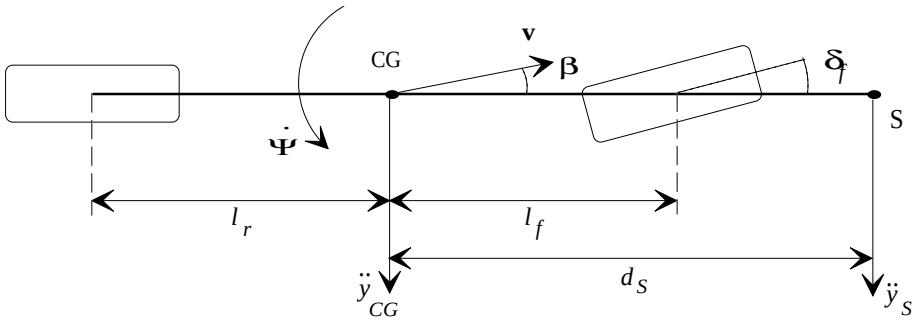

Fig. 1: Single-track model for car steering

The analysis in later sections is based on parameters of one of the cars used in the California PATH project, a 1986 Pontiac 6000 STE sedan, summarized in Table 1.

M	I_Ψ	ℓ_f	ℓ_r	d_S	$c_f = c_r$
1573 kg	2873 kg m^2	1.1 m	1.58 m	1.96 m	80000 N/rad

Table 1: Car parameters of a 1986 Pontiac 6000 STE sedan

The transfer function from the steering angle δ_f to side slip angle β is given by

$$\beta(\boldsymbol{s}) = \frac{(\mu c_f I_\Psi v)\boldsymbol{s} + \mu c_f \ell_f (\mu c_r \ell - M v^2)}{\mathcal{D}(\boldsymbol{s})} \delta_f(\boldsymbol{s}), \tag{2}$$

where $\mathcal{D}(\boldsymbol{s})$ is the second order denominator

$$\begin{aligned} \mathcal{D}(\boldsymbol{s}) &= I_\Psi M v^2 \boldsymbol{s}^2 + \mu v \left(I_\Psi (c_f + c_r) + M(c_f \ell_f^2 + c_r \ell_r^2) \right) \boldsymbol{s} + \\ &\quad \mu M v^2 (c_r \ell_r - c_f \ell_f) + \mu^2 c_f c_r \ell^2. \end{aligned} \tag{3}$$

The *Laplace*-variable is denoted by $\boldsymbol{s}$. The dynamics of yaw rate $\dot{\Psi}$ are

$$\begin{aligned} \dot{\Psi}(\boldsymbol{s}) &= \frac{(\mu c_f \ell_f M v^2)\boldsymbol{s} + \mu^2 c_f c_r \ell v}{\mathcal{D}(\boldsymbol{s})} \delta_f(\boldsymbol{s}), \\ &= \frac{1}{\boldsymbol{s}} W(\boldsymbol{s}) \delta_f(\boldsymbol{s}), \end{aligned} \tag{4}$$

where $W(\boldsymbol{s})$ denotes the yaw acceleration transfer function

$$\ddot{\Psi}(\boldsymbol{s}) = W(\boldsymbol{s}) \delta_f(\boldsymbol{s}). \tag{5}$$

Defining lateral acceleration at CG as an output of the system (1), a transfer function can be derived as

$$\begin{aligned} \ddot{y}_{CG}(\boldsymbol{s}) &= \frac{\mu c_f v^2 I_\Psi \boldsymbol{s}^2 + \mu^2 c_f c_r \ell \ell_r v \boldsymbol{s} + \mu^2 c_f c_r \ell v^2}{\mathcal{D}(\boldsymbol{s})} \delta_f(\boldsymbol{s}) \\ &= V_{CG}(\boldsymbol{s}) \delta_f(\boldsymbol{s}). \end{aligned} \tag{6}$$

At displacement sensor S, lateral acceleration $\ddot{y}_S$ comprises lateral acceleration at CG and yaw acceleration scaled by look-ahead distance d_S:

$$\begin{aligned} \ddot{y}_S(\boldsymbol{s}) &= \ddot{y}_{CG}(\boldsymbol{s}) + d_S \ddot{\Psi}(\boldsymbol{s}) \\ &= \frac{\mu c_f v^2 \left(M \ell_f d_S + I_\Psi \right) \boldsymbol{s}^2 + \mu^2 c_f c_r \ell v \left(d_S + \ell_r \right) \boldsymbol{s} + \mu^2 c_f c_r \ell v^2}{\mathcal{D}(\boldsymbol{s})} \delta_f(\boldsymbol{s}) \\ &= (V_{CG}(\boldsymbol{s}) + d_S \, W(\boldsymbol{s})) \delta_f(\boldsymbol{s}) \\ &= V_S(\boldsymbol{s}) \delta_f(\boldsymbol{s}). \end{aligned} \tag{7}$$

For look-down systems, the lateral displacement sensor is usually located at the front bumper and look-ahead distance d_S is approximately half the car length. The front wheel steering angle δ_f is the output of a position controlled actuator with limited bandwidth, denoted by

$$\delta_f(\boldsymbol{s}) \quad = \quad A(\boldsymbol{s})\,\delta(\boldsymbol{s}), \tag{8}$$

where δ is the commanded steering angle.

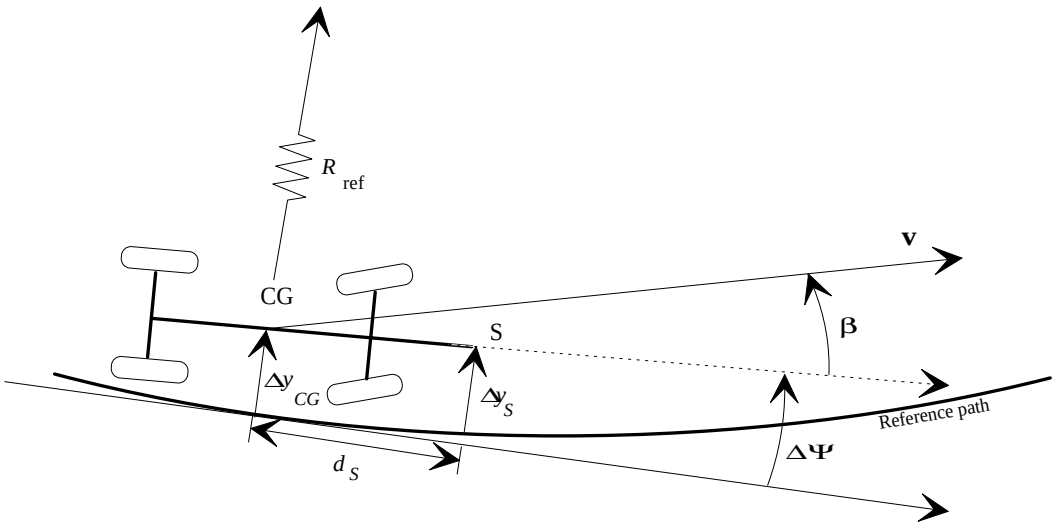

Fig. 2: Vehicle following a reference path

Fig. 2 shows a vehicle following a circular reference path with a radius R_{ref}. Lateral displacement of the vehicle from the reference path is denoted Δy_{CG} at CG and Δy_S at sensor location S. California highways consist of circular arcs matched together without transitions. The vehicle longitudinal axis spans the sideslip angle β with the vehicle velocity vector $\mathbf{v}$ and the angular displacement error $\Delta\Psi$ with the tangent to the reference path. For convenience, we define the reference curvature as $\rho_{\text{ref}} := \dfrac{1}{R_{\text{ref}}}$.

From above, we extract the plant subsystems: a kinematic subsystem (I), a geometric road reference subsystem (II), and the lateral vehicle force generation (III) in (7) with actuator dynamics (IV) in (8), all viewed at the sensor location S. The reference subsystem prescribes the desired lateral acceleration at S,

$$\ddot{y}_{\text{ref}}(\boldsymbol{s}) \quad = \quad v^2 \rho_{\text{ref}}(\boldsymbol{s}),$$

where ρ_{ref} is the road reference curvature at S. The kinematic subsystem reduces to a double integrator for the lateral displacement measurement Δy_S:

$$\Delta y_S(\boldsymbol{s}) \quad = \quad \frac{1}{\boldsymbol{s}^2}(\ddot{y}_S(\boldsymbol{s}) - \ddot{y}_{\text{ref}}(\boldsymbol{s})). \tag{9}$$

A block diagram of the closed loop with controller $C(\boldsymbol{s})$ using output feedback of Δy_S is shown in Fig. 3.

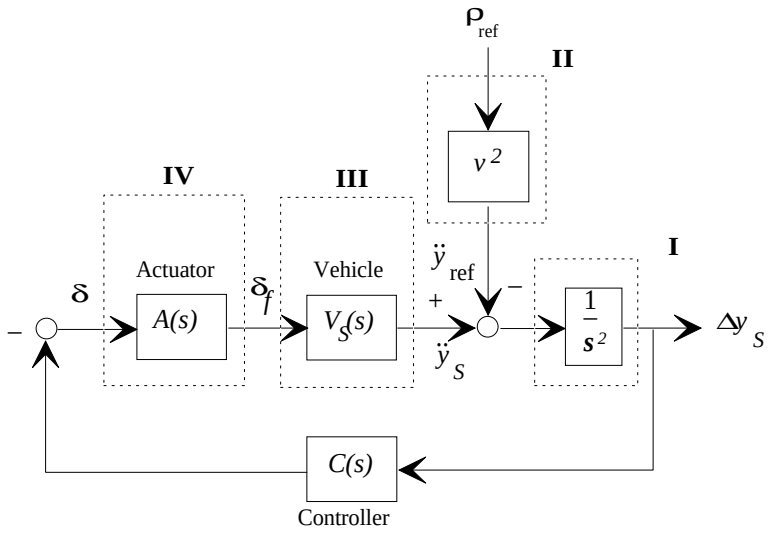

Fig. 3: Block diagram of an output feedback steering control system

2.2 Performance requirements

Human driving performance readily adapts to traffic situations. In heavy traffic and on narrow lanes, e.g. near construction sites, drivers concentrate on lane keeping with small errrors. On wide, open highways, however, concentration decreases and so does the tracking performance. The total width of passenger cars including side-mirrors may vary within 1.8-2.4 m (approx. 6-8 ft) from subcompacts to full-size vans and pick-ups. US highway lanes have a width of 3.6 m (approx. 12 ft), leaving a worst-case margin of 0.6 m (approx. 2 ft) on each side for lane keeping errors.

An automatic steering system is expected to achieve tight tracking performance [27] to allow for sufficient safety margins in case of emergencies. Assuming a one-to-one proportioning between margins for normal conditions and for emergency situations like tire bursts [28], a maximum error of 0.3 m (approx. 1 ft) for normal conditions and for emergencies, respectively, appears reasonable. For normal conditions, this error is further subdivided into nominal operation and extreme situations. Hence a nominal maximum error of 0.15 m (approx. $\frac{1}{2}$ ft) and an extreme situation maximum error of 0.3 m (approx. 1 ft) are used as performance requirement in this study.

The nominal reference input of an automatic steering system is the road curvature ρ_{ref}. (Disturbances include wind gusts, pot holes etc.) The vehicle speed $v = |\mathbf{v}|$ should be chosen to limit the lateral acceleration a_{ref} during steady state curve riding to $(a_{\text{ref}})_{\max} = 0.2\,\text{g}$,

where $g = 9.81$ m/s^2 is the gravity constant. We assume that vehicle speed v is adjusted according to the respective curvature of a specific stretch of road with

$$v^2 = \frac{(a_{\text{ref}})\max}{(\rho_{\text{ref}})\max}. \tag{10}$$

Under normal highway driving conditions, the lateral error should not exceed $|\Delta y_S| = 0.15$ m, e.g. for a step input (10). Extreme situations, which would allow for maximum lateral errors of 0.3 m include significant simultaneous changes of road adhesion μ, concurrent strong braking/accelerating, and steps from left maximum curvature to right maximum curvature or vice-versa without intermediate straight segments.

Ride comfort is an important concern for automatic steering control design. Human passengers are likely to reject automatically steered vehicles, and AHS as a whole, if the ride comfort is inferior to manual driving. Research in comfort for automobiles so far has focused on suspensions. A few concepts, however, carry over to steering control and can be translated into performance requirements.

Comfort is mainly constituted by the acceleration acting on the passenger. More than the magnitude of acceleration, its rate, also called jerk, determines the comfort level of riders. A continuous, steady state acceleration up to 0.3-0.4 g can be comfortably counteracted by humans. Sudden changes in lateral acceleration, however, may cause a feeling of discomfort. For one, acceleration components in the 5-10 Hz frequency range can excite internal body resonances, without the effected person being able to allocate the cause of discomfort.

For deriving consequences for lateral control design from above, consider Fig. 3. When closing the control loop from measurement Δy_S to δ via a controller $C(\boldsymbol{s})$, reference acceleration $\ddot{y}_{\text{ref}}$ is to be matched by $\ddot{y}_S$ without excessive overshoot. To fulfill the discussed frequency constraints, the bandwidth of the closed loop transfer function from $\ddot{y}_{\text{ref}}$ to $\ddot{y}_S$ should be below 5 Hz, but may exceed the approx. 1 Hz human reaction time since significant steps in road reference curvature are usually rare. Furthermore, the effects of steps in $\ddot{y}_{\text{ref}}$ can be decreased by previewing road curvature for a feedforward term in the steering controller.

2.3 Practical constraints

An additional practical constraint relating to comfort is system noise, the main source being lateral displacement sensor S. Assuming white sensor noise, no frequency above approx. 0.1-0.5 Hz should be amplified extraordinarily in the path to lateral acceleration $\ddot{y}_S$. Good damping in the closed loop is required for suppressing uncomfortable lateral acceleration and jerk. A reasonable compromise is to require an automatic steering feedback loop to have at least a similar amount of damping as the conventional, manually steered car. Furthermore,

high frequency noise in lateral displacement measurement Δy_S should not be allowed to propagate through the controller $C(\boldsymbol{s})$ to the input δ of steering actuator $A(\boldsymbol{s})$ to avoid mechanical wear, requiring roll-off in the controller beyond the designated cross-over frequency.

The contradicting performance requirements of maximum lateral error and comfort have to be achieved under a wide range of operating conditions. Most plant parameters like car mass and inertia, and location of CG are slowly time varying and can be estimated on-line by appropriate algorithms. These parameters as listed in Table 1 for a sample car are assumed to be known for the remainder of this study. Only the road adhesion factor μ is assumed unknown within its range of uncertainty. The physical upper bound is $\mu = 1$ for dry road with a good surface. Empirical data of various studies suggests $\mu \approx 0.5$ for wet (slippery) road and a lower bound of $\mu = 0.1$ for pure ice. Since changes may be abrupt, stability has to be guaranteed *robustly* without adaptation, at least for sets of the above range.

A set of 'normal' road conditions is defined for this study as $0.5 \leq \mu \leq 1$ for wet or better road. This range is chosen conservatively to include different road surface and tire qualities with varying adhesion factors. 'Adverse' road conditions, e.g. snow and ice, are not considered explicitly here. On one hand, it is assumed that such extreme conditions would either lead to discontinued operation of automated highways or to significant speed reductions. On the other hand, the analysis presented in the sequel can be easily extended to more extreme conditions.

Two major implementational design constraints have to be considered. The first constraint is related to the steering actuator dynamics. The necessity of being able to implement an automatic steering system on an average passenger car without major constructional modification of currently used steering mechanisms limits the available actuator bandwidth. Cost and power considerations impose bandwidth limitations of maximum 10 Hz on a position-controlled, third or higher order steering actuator, regardless whether it is electric or hydraulic.

The actuator bandwidth is subject to uncertainty due to operating conditions like temperature and command amplitude. A worst-case bandwidth of 5 Hz proved realistic in the experiments performed at California PATH. Compared with a human driver (below 1 Hz) and the car dynamics (about 1 Hz), the bandwidth limitations constitue a serious factor, considering the discussed performance, comfort and robustness requirements. Furthermore, the inherent uncertainty of the actuator dynamics imply that the steering controller has to provide roll-off itself, taking into account the worst-case actuator dynamics.

3 Problem Analysis

A thorough system analysis is based on an appropriate degree of abstraction for highlighting the key characteristics and on utilization of multiple angles of view for describing the problem.

For this study, we chose various tools of linear systems theory to examine the plant and the controller design requirements. The discussion in this section is founded entirely on linear system theory. Using the linearized model of Section 2.1, a linear control design is viewed as the basis for a possibly more involved design using nonlinear techniques. Any nonlinear controller, however, can be linearized around an operating point, e.g. $\Delta y_S = 0$ for any μ and v. The linearized version of a nonlinear controller must of course satisfy all stability requirements and should at least partially fulfill the performance requirements given in Section 2.2, under the practical constraints of Section 2.3. Note that this holds both for analytical nonlinear techniques like sliding mode control and for more heuristic methods like fuzzy and neural-network control.

Any controller, linear or nonlinear, will rely on the available information content of the feedback signal(s). We argue that basic systems theory considerations, without using a specific control design methodology, are sufficient, if not required, to understand the fundamental problems of automatic steering control. Later, refinement of the controller will be aided by modern tools of control design. To some extend, the fundamental problem of automatic steering control under practical conditions has been underestimated in the past, partly due to the lack of a detailed system analysis. In particular, automatic steering of vehicles driving at highway speed with look-down systems needs concurrent consideration of all performance requirements and practical constraints already at the system analysis and control design stage.

The block diagram in Fig. 3 shows that the double integrator (9) is to be controlled via the lateral vehicle acceleration $\ddot{y}_S$, based on displacement measurement Δy_S, and with input $\ddot{y}_{\text{ref}}$. The open loop characteristics $G(\boldsymbol{s})$, obtained by combining controller $C(\boldsymbol{s})$, vehicle lateral acceleration $V_S(\boldsymbol{s})$ in (7), and actuator $A(\boldsymbol{s})$ in (8), are written as

$$G(\boldsymbol{s}) \;=\; C(\boldsymbol{s})A(\boldsymbol{s})V_S(\boldsymbol{s}) \tag{11}$$

and constitutes the 'control' for the 'plant' $\left(\frac{1}{\boldsymbol{s}^2}\right)$. The closed loop input-output relationship between road curvature ρ_{ref} and lateral displacement Δy_S is denoted by

$$\begin{aligned} \Delta y_S &= \frac{v^2}{\boldsymbol{s}^2 + G(\boldsymbol{s})}\rho_{\text{ref}}, \\ &= H(\boldsymbol{s})\rho_{\text{ref}}. \end{aligned} \tag{12}$$

Using multiple perspectives, the following subsections concurrently analyze plant dynamics and resulting control synthesis requirements to obtain suitable $G(\boldsymbol{s})$. First, step responses are employed to give a flavor of the vehicle dynamics and their variation with vehicle speed and road adhesion μ. Second, Bode diagrams are used for frequency domain analysis to pinpoint the dominant vehicle characteristics. Third, these characteristics are traced back to the pole/zero locations in eigenvalue plane. Last, and most ambitious, a physical interpretation is offered to enhance the overall understanding and to motivate the control design directions for $G(\boldsymbol{s})$ in Section 4.

3.1 Time Domain Analysis

The analysis commences with a set of illustrative step responses with zero initial conditions shown in Fig. 4. In the top two plots, the dependency of lateral vehicle acceleration $\ddot{y}_{CG}(t)$ at CG (6) on speed v (left plots) and on road adhesion μ (right plots) is depicted for steering angle steps of $\delta_f = 0.01\,\mathrm{rad}$, neglecting the actuator dynamics $A(\boldsymbol{s})$ in (8). The two plots in the bottom row show the associated yaw rate responses $\dot{\Psi}(t)$.

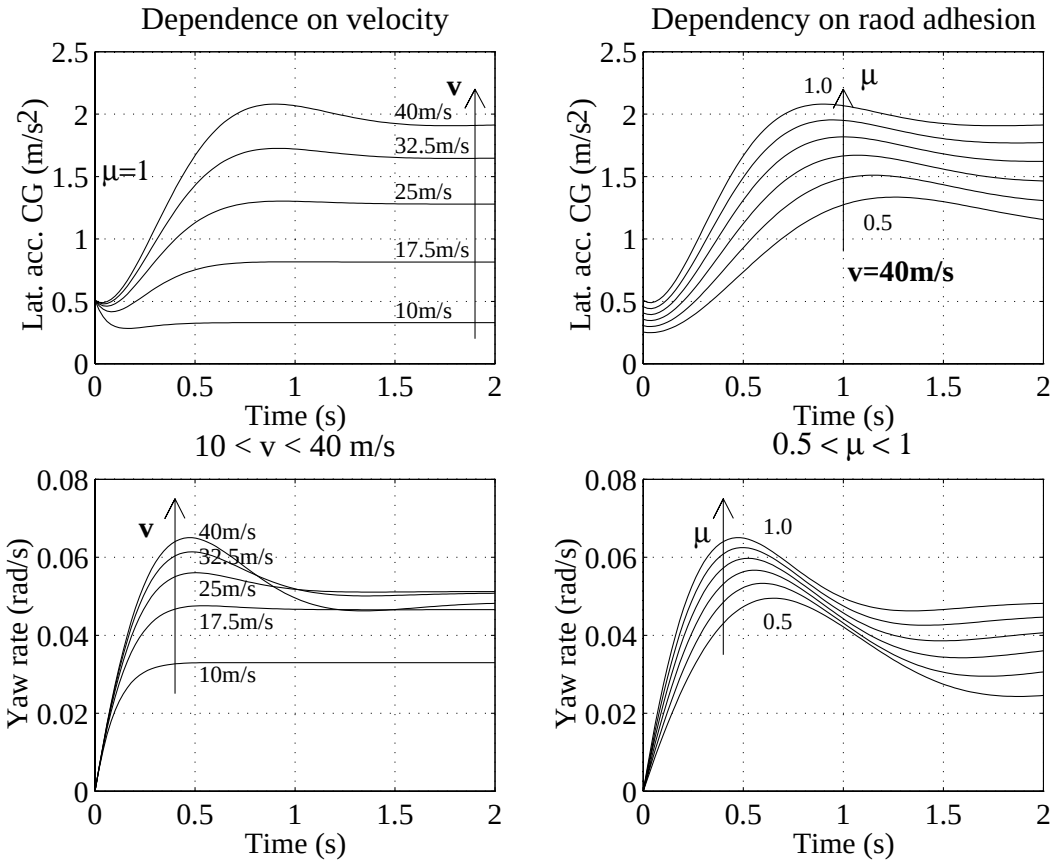

Fig. 4: Step responses of lateral acceleration $\ddot{y}_{CG}(t)$ at CG (top row) and yaw rate $\dot{\Psi}(t)$ (bottom row) for variation of speed v within $10\,\mathrm{m/s} \leq v \leq 40\,\mathrm{m/s}$ on good road $\mu = 1$ (left column) and for variation of road adhesion $0.5 \leq \mu \leq 1$ at high speed $v = 40\,\mathrm{m/s}$ (right column)

Observations

- The *lateral acceleration* transfer function $\ddot{y}_{CG}(t)$ has a direct throughput, i.e. zero difference degree in second order (6).

- The initial value $\ddot{y}_{CG}(0)$ is speed independent, but varies linearly in μ, whereas steady state $\ddot{y}_{CG}(\infty) = \lim_{t\to\infty} \ddot{y}_{CG}(t)$ is both speed and μ-dependent.
- For low speed, the initial value $\ddot{y}_{CG}(0)$ exceeds steady state $\ddot{y}_{CG}(\infty)$, featuring a transient without overshoot and oscillations.
- At higher speeds, the initial value is considerably smaller than steady state, and the transient is subject to increasing overshoot and oscillatory behavior.
- *Yaw rate* $\dot{\Psi}(t)$ follows second order transfer function (4) with first order numerator, i.e. difference degree one.
- Steady state $\dot{\Psi}(\infty)$ increases significantly from $v = 10\,\mathrm{m/s}$ to $v = 20\,\mathrm{m/s}$, but only slightly from there on for higher speeds. However, steady state $\dot{\Psi}(\infty)$ depends almost linearly on road adhesion μ.
- For increasing speed and degrading road quality, yaw rate step responses tend to overshoot and oscillate, even more so than lateral acceleration.

Consequences for control

At low speed, the vehicle dynamics are well-behaved without overshoot and oscillations. An initial value of lateral acceleration $\ddot{y}_{CG}(0)$ at CG exceeding steady state $\ddot{y}_{CG}(\infty)$ for a step input of steering angle δ_f indicates a gain increase of $V_{CG}(\boldsymbol{s})$ for increasing frequencies. The influence of road adhesion μ on the vehicle dynamics is negligible, geometric kinematics prevail (not shown here explicitly, see [22]).

Increasing speed leads to increasing oscillatory behavior and significant overshoot, both in lateral acceleration $\ddot{y}_{CG}(t)$ and in yaw rate $\dot{\Psi}(t)$ step responses. The steady state value $\ddot{y}_{CG}(\infty)$ increases with v and exceeds significantly the initial value $\ddot{y}_{CG}(0)$ for higher speed, indicating a gain drop in $V_{CG}(\boldsymbol{s})$ and associated phase lag. The increased overshoot and the tendency to oscillate indicates an increasing influence of the zeros in the transfer functions and decreased damping of the vehicle pole-pair in (3). Furthermore, an almost linear dependency on μ of both lateral acceleration and yaw rate is visible in the right two plots of Fig. 4 for $v = 40\,\mathrm{m/s}$.

3.2 Frequency Domain Analysis

We continue the analysis using Bode diagrams. Frequency domain most clearly reveals the general structure of the vehicle dynamics and resulting controller requirements. A set of Bode diagrams of the lateral vehicle dynamics $V_{CG}(\boldsymbol{s})$ at CG is shown in Fig. 5. The left diagram illustrates the dependency of $V_{CG}(\boldsymbol{s})$ on driving speed v for the range $10\,\mathrm{m/s} \leq v \leq 40\,\mathrm{m/s}$

on a dry road with good surface $\mu = 1$. The right diagram depicts the changes caused by variation of road adhesion μ from poor conditions $\mu = 0.5$ to good conditions $\mu = 1$ at speed $v = 40\,\mathrm{m/s}$. Note that the actuator dynamics $A(\boldsymbol{s})$ in (8) have not been included.

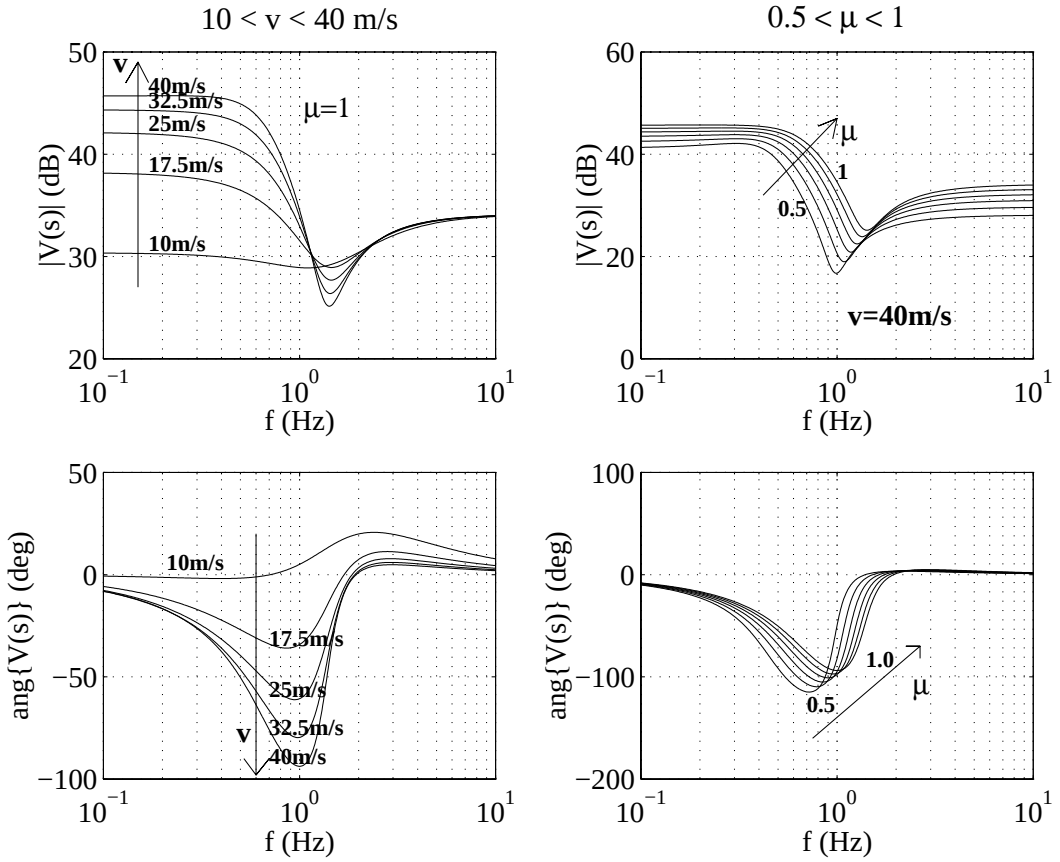

Fig. 5: Lateral acceleration dynamics $V_{CG}(\boldsymbol{s})$ at CG for variation of speed within $10\,\mathrm{m/s} \leq v \leq 40\,\mathrm{m/s}$ on good road $\mu = 1$ (left Bode diagram) and for variation of road adhesion $0.5 \leq \mu \leq 1$ at high speed $v = 40\,\mathrm{m/s}$ (right Bode diagram)

Observations

- Lateral acceleration dynamics $V_{CG}(\boldsymbol{s})$ have notch characteristics with a distinct natural mode around 0.5-2 Hz.
- For low speed, the steady state gain

$$V_{CG}(0) \;=\; \frac{\mu c_f c_r \ell v^2}{M v^2 (c_r \ell_r - c_f \ell_f) + \mu c_f c_r \ell^2} \tag{13}$$

  is smaller than the high frequency gain

$$V_{CG}(\infty) \;=\; \lim_{j\omega \to \infty} |V_{CG}(j\omega)| \;=\; \frac{\mu c_f}{M}. \tag{14}$$

The overall gain *increase* from $V_{CG}(0)$ to $V_{CG}(\infty)$ for $v \leq 14\,\mathrm{m/s}$ provides phase lead in the range of the natural mode and leads to step responses with initial values exceeding steady state, recall Fig. 4.

- For increasing speed, steady state gain $V_{CG}(0)$ increases strongly with v while high frequency gain $V_{CG}(\infty)$ remains constant. The gain *drop* from $V_{CG}(0)$ to $V_{CG}(\infty)$ for $v > 14\,\mathrm{m/s}$ leads to significant phase lag in the range of $0.1 - 2\,\mathrm{Hz}$. This corresponds to initial values $\ddot{y}_{CG}(0)$ being smaller than steady state $\ddot{y}_{CG}(\infty)$ in the top row of Fig. 4.

- At higher speeds, the natural mode is accompanied by a gain "undershoot" around $1 - 2\,\mathrm{Hz}$.

- Decreasing road adhesion μ decreases the gain $|V_{CG}(\jmath\omega)|$ at all frequencies, also visible in the step responses in Fig. 4 (right column). Furthermore, the frequency of the natural mode decreases with deteriorating road adhesion.

- The gain variation of $V_{CG}(s)$ due to μ increases with speed as shown in [22]. In particular, a step from $\mu = 1$ to $\mu = 0.5$ leads to an approximate 10% gain drop of $V_{CG}(0)$ at $v = 10\,\mathrm{m/s}$, but to an approximate gain drop of 40% at $v = 40\,\mathrm{m/s}$. The increasing dependency of the gain $|V_{CG}(\boldsymbol{s})|$ on μ for higher speeds complicates the robustness problem with respect to changes of μ as discussed in Section 2.3.

Viewed at a location S, the lateral vehicle acceleration has an embedded additional yaw acceleration component. According to (7), lateral acceleration $\ddot{y}_S$ at S is a linear combination of lateral acceleration $\ddot{y}_{CG}$ at CG and yaw acceleration $\ddot{\Psi}$, with the weight of the latter being d_S. A set of Bode diagrams for the yaw acceleration transfer function $W(\boldsymbol{s})$ in (5) is shown in Fig. 6 for similar conditions as in Fig. 5.

Note that $V_{CG}(\boldsymbol{s})$ and $W(\boldsymbol{s})$, and hence $V_S(\boldsymbol{s})$ share denominator $\mathcal{D}(\boldsymbol{s})$ in (3), but have different numerators. In particular, yaw acceleration $W(\boldsymbol{s})$ has differentiating low frequency characteristics with associated phase lead, up to a corner frequency ω_c. The gain in the low frequency region depends linearly on speed v, whereas the high frequency gain is speed independent. Furthermore, the natural mode is less markable in $W(\boldsymbol{s})$ than in $V_{CG}(\boldsymbol{s})$, hinting that the zero-pair in lateral acceleration rather than the pole-pair causes the gain undershoot in the $1 - 2\,\mathrm{Hz}$ region of $V_{CG}(\boldsymbol{s})$.

Linear combination of $V_{CG}(\boldsymbol{s})$ and $W(\boldsymbol{s})$ to form $V_S(\boldsymbol{s})$ in (7) is not straightforward in frequency domain. We restrict the following discussion to qualitative arguments: In the low frequency range, the magnitude of $V_{CG}(\boldsymbol{s})$ exceeds that of $W(\boldsymbol{s})$, leading to dominance of $V_{CG}(\boldsymbol{s})$ in $V_S(\boldsymbol{s})$. At some frequency ω_e, depending on d_S, the magnitudes $|V_{CG}(\jmath\omega)|$ and $(d_S|W(\jmath\omega)|)$ become comparable, implying that both transfer functions contribute to $V_S(\boldsymbol{s})$ according to their exact respective weight.

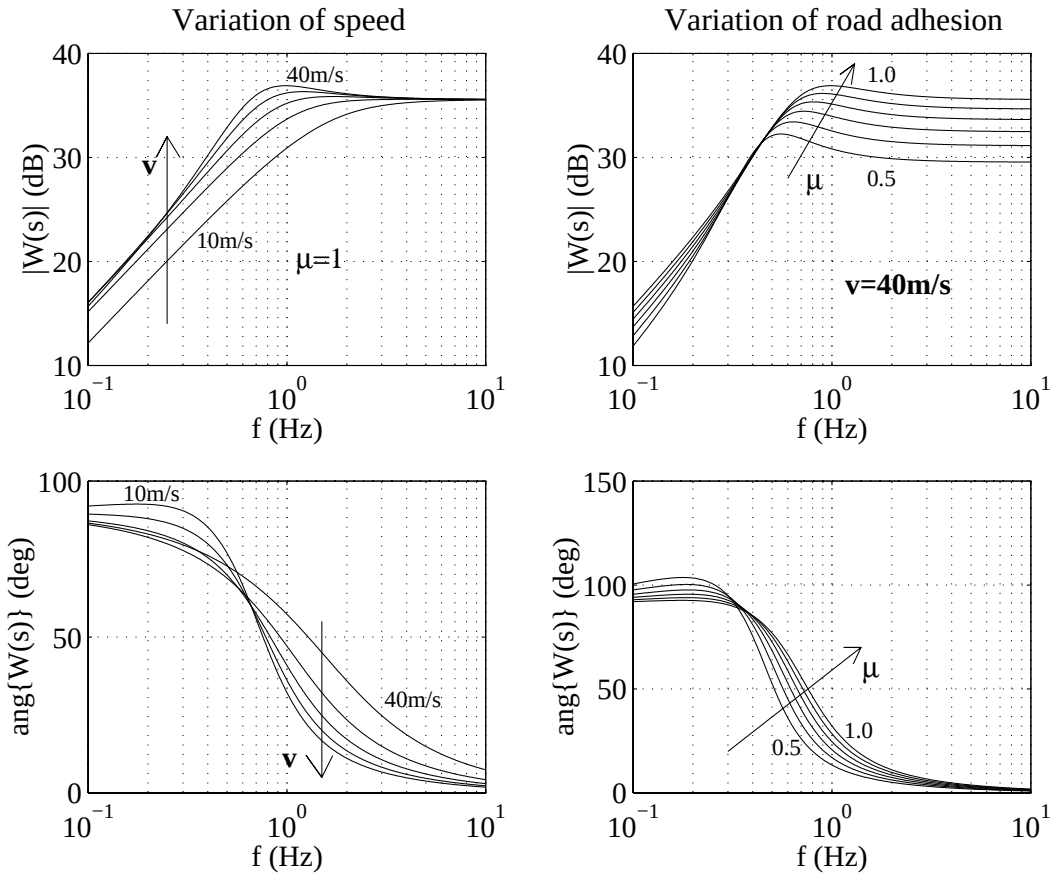

Fig. 6: Yaw acceleration dynamics $W(\boldsymbol{s})$ for variation of speed within $10\,\mathrm{m/s} \leq v \leq 40\,\mathrm{m/s}$ on good road $\mu = 1$ (left Bode diagram) and for variation of road adhesion $0.5 \leq \mu \leq 1$ at high speed $v = 40\,\mathrm{m/s}$ (right Bode diagram)

Observations

- The steady state gain of $V_S(\boldsymbol{s})$ is solely determined by lateral acceleration at CG, i.e.

$$\begin{aligned} V_S(0) &= \frac{\mu c_f c_r \ell v^2}{M v^2 (c_r \ell_r - c_f \ell_f) + \mu c_f c_r \ell^2} \\ &= V_{CG}(0) \end{aligned} \tag{15}$$

  in (13), with strong depedency on speed v.

- The high frequency gain of $V_S(\boldsymbol{s})$ is velocity independent, but varies linearly with d_S,

$$\begin{aligned} V_S(\infty) &= \lim_{j\omega \to \infty} |V_S(j\omega)| \\ &= \mu c_f \left(\tfrac{1}{M} + \tfrac{d_S \ell_f}{I_\Psi} \right) \\ &= V_{CG}(\infty) + d_S W(\infty) \end{aligned} \tag{16}$$

- The frequency ω_e with $|V_{CG}(\jmath\omega_e)| = |W(\jmath\omega_e)|$ depends both on v and d_S. Since low frequency $V_{CG}(\jmath\omega)$ varies with almost quadratic v^2, but low frequency $W(\jmath\omega)$ depends less than linearly on speed v, compensation of the gain changes due to speed requires an approximately linear increase of d_S with v in (7). Note that the phase lag in $V_{CG}(\jmath\omega)$ is only compensated by phase lead in $W(\jmath\omega)$ for $\omega_e < \omega < \omega_c$, requiring sufficiently large look-ahead d_S due to fixed corner frequency ω_c.

Obviously, look-ahead distance d_S plays a decisive role in weight distribution in (7), and in particular in determining phase lead or lag in the range of the natural mode. This influence of look-ahead distance d_S is illustrated in Fig. 7. Left, Bode diagrams for a short look-ahead distance of $d_S = 2\,\mathrm{m}$, typical for look-down reference systems, are depicted for good, dry road ($\mu = 1$) and different speeds $10 \leq v \leq 40\,\mathrm{m/s}$. Right, a high speed situation ($v = 40\,\mathrm{m/s}$, $\mu = 1$) is shown for various look-ahead distances $0 \leq d_S \leq 10\,\mathrm{m}$. As predicted above, phase lag in the range $0.1 - 1\,\mathrm{Hz}$ increases for increasing speed when using a look-down reference system with fixed $d_S = 2\,\mathrm{m}$ (left Bode diagram). Conversely, increasing d_S decreases phase lag and eventually provides phase lead even at high speeds (right Bode diagram). Not surprisingly, this complies with human driving behavior, where the look-ahead distance is adjusted approximately proportional to speed.

Consequences for control

For look-down reference systems with small d_S, the phase lag around the natural mode has significant consequences for control design. One of the key problems is that the natural mode of the vehicle is in the frequency range needed for stabilization, due to performance requirements. In order to achieve a maximum error of $|(\Delta y_S)_{\max}| \leq 0.15\,\mathrm{m}$ for a step in road curvature of $|\Delta\rho_{\mathrm{ref}}| = 0.2g/v^2$, a minimum low frequency gain of the controller is required. The minimum gain requirement leads to a minimum requirement for the cross-over frequency, colliding with the frequency of the natural mode of the vehicle dynamics, and for higher speed, also with the actuator dynamics.

The performance requirement for 'normal' operation of less than $|(\Delta y_S)_{\max}| \leq 0.15\,\mathrm{m}$ error for a step input in road curvature of $(\Delta\rho_{\mathrm{ref}})_{\max})$ in (10) translates into a gain requirement for the closed loop transfer function $H(\boldsymbol{s})$ in (12),

$$|H(\boldsymbol{s})| \;\leq\; \frac{|(\Delta y_S)_{\max}|}{|(\Delta\rho_{\mathrm{ref}})_{\max}|}, \qquad \forall \boldsymbol{s}. \tag{17}$$

This estimation is based on the inequality

$$|\Delta y_S(t)| \;=\; |\mathcal{L}^{-1}\left\{H(\boldsymbol{s})\frac{1}{\boldsymbol{s}}\,(\Delta\rho_{\mathrm{ref}})_{\max}\right\}| \;\leq\; |H(\boldsymbol{s})| \cdot |(\Delta\rho_{\mathrm{ref}})_{\max}|, \tag{18}$$

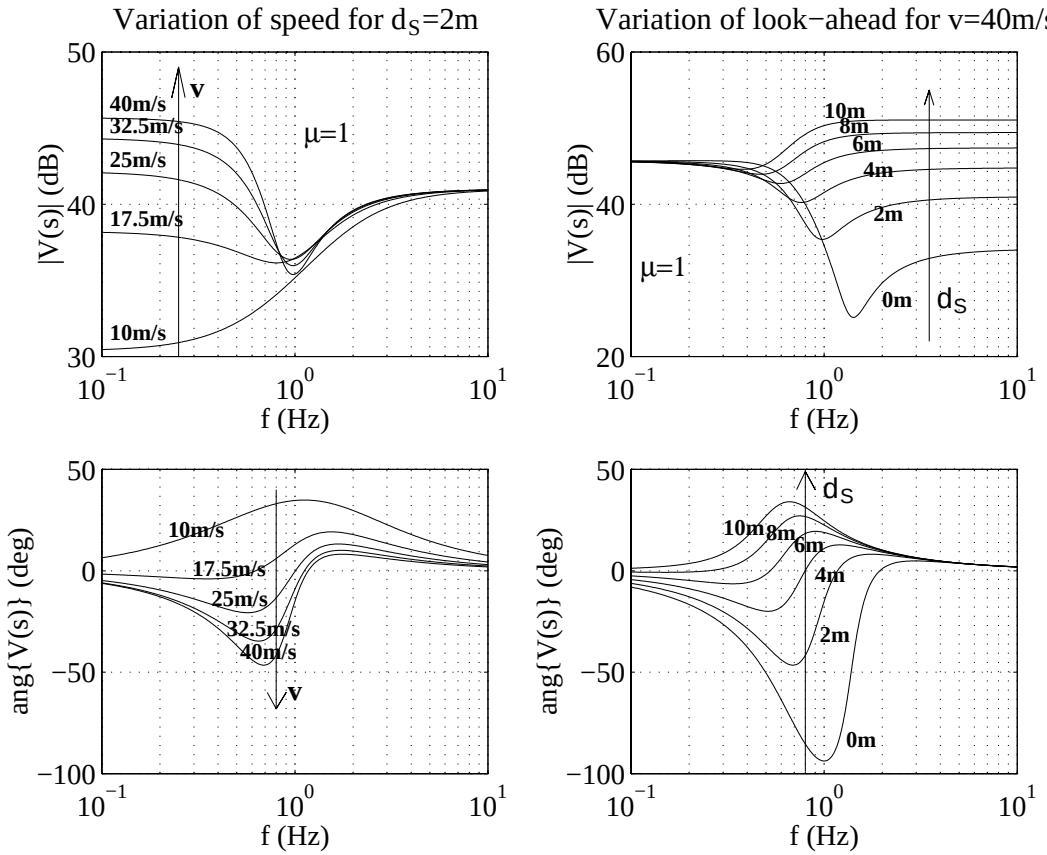

Fig. 7: Lateral acceleration dynamics $V_S(\boldsymbol{s})$ at sensor location S, $d_S = 2\,\mathrm{m}$ in front of CG, for variation of speed within $10\,\mathrm{m/s} \leq v \leq 40\,\mathrm{m/s}$ on good road $\mu = 1$ (left Bode diagram) and for variation of look-ahead $0 \leq d_S \leq 10\,\mathrm{m}$ for $\mu = 1$ at high speed $v = 40\,\mathrm{m/s}$ (right Bode diagram)

where $\mathcal{L}^{-1}\{\cdot\}$ denotes the inverse *Laplace*-transform. Substituting open loop $G(\boldsymbol{s})$ in (11) into closed loop $H(\boldsymbol{s})$ in (12) yields

$$H(\boldsymbol{s}) \;=\; \frac{v^2}{\boldsymbol{s}^2 + C(\boldsymbol{s})A(\boldsymbol{s})V_S(\boldsymbol{s})}, \tag{19}$$

with $V_S(\boldsymbol{s})$ denoting the lateral car dynamics at sensor location S in (7), $A(\boldsymbol{s})$ describing the actuator dynamics (8), and $C(\boldsymbol{s})$ being the controller to be designed. Note that the quadratic dependency of $H(\boldsymbol{s})$ on speed v^2 is compensated by the inverse quadratic speed dependency of $(\Delta\rho_{\mathrm{ref}})_{\max}$ in (10) with speed independent $(a_{\mathrm{ref}})_{\max}$.

An output feedback controller $C(\boldsymbol{s})$, relying on measurement of lateral displacement Δy_S, has to compensate the phase lag in vehicle dynamics $V_S(\boldsymbol{s})$ and additionally to provide sufficient phase margin for stabilisation of the double integrator. The gain and phase requirements for controller $C(\boldsymbol{s})$ can be examined by solving (19) for $C(\boldsymbol{s})$ under constraint

(17). This performance constraint should be coupled with the stability constraint as shown in Fig. 8 for $v = 40\,\mathrm{m/s}$, $\mu = 1$, and $d_S = 2\,\mathrm{m}$.

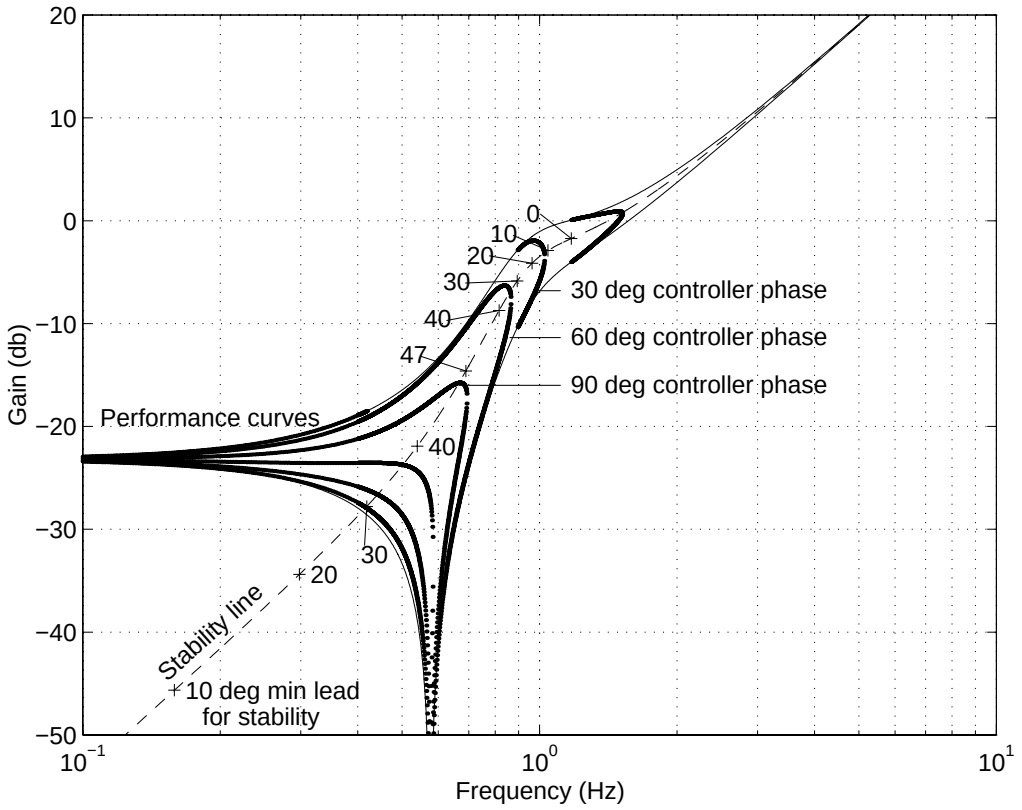

Fig. 8: Requirements for controller $C(\boldsymbol{s})$ at $v = 40\,\mathrm{m/s}$, $\mu = 1$, and with $d_S = 2\,\mathrm{m}$ in terms of gain and phase at the critical frequency range for achieving the desired performance

Performance curves, the solutions of the above performance constraint for $|C(\boldsymbol{s})|$ and various values of $\angle C(\boldsymbol{s})$, are displayed for the parameters of the Pontiac 6000 STE sedan of Table 1. The performance constraint dictates that at any frequency, $|C(\boldsymbol{s})|$ should lie above the performance curve corresponding to the respective $\angle C(\boldsymbol{s})$. Similarly, the stability requirement dictates $\angle C(\boldsymbol{s})$ to be at least the marked value at cross-over, when $|C(\boldsymbol{s})|$ intersects the stability line (inverse plant). In order to guarantee good damping and a sufficient phase margin, $\angle C(\boldsymbol{s})$ should exceed the marked value by at least 50^o at cross-over. This already stringent constraint on the control design is aggrevated by the requirement of controller roll-off immediately after the cross-over frequency, but within the actuator bandwidth of approx. 5 Hz. Both the controller low-pass for roll-off and the actuator dynamics start introducing phase lag from around 2 Hz.

The controller $C(\boldsymbol{s})$ should avoid excessive phase lead in the vicinity of actuator dynamics since this could cause the actuator to saturate, with consequent harmful and possibly unsta-

ble limit cycles. In addition to actuator constraints, high controller gains at high frequencies are extremely undesirable due to noise considerations. As is obvious from Fig. 8, much lower gain sufficies in the low frequency range to achieve the desired performance. High gain at high frequencies amplifies the noise in measurement Δy_S, leading to poor comfort and also to high wear of mechanical parts in the steering mechanism.

The controller requirements shown in Fig. 8 are already highly demanding for a single speed and constant (known) road adhesion μ. Addition of the robustness requirement of simultaneous stability and good performance for $0.5 \leq \mu \leq 1$ further complicates matters. Variation of μ introduces a 40% variation in vehicle gain $|V_S(\jmath\omega)|$ (see [22]) and shifts the frequency of the natural mode. In order to satisfy the performance requirements, the gain variation has to be compensated by increasing the low frequency gain of controller $C(\boldsymbol{s})$. The increasing phase lag of vehicle dynamics $V_S(\boldsymbol{s})$ for decreasing μ requires even more phase lead by the controller. Most important, however, the phase lead region of the controller has to sustain for a significant frequency range, since cross-over frequency varies concurrently to variation of gain and natural mode in $V_S(\boldsymbol{s})$ due to changing μ. An additional gain increase results for higher frequencies, further increasing system bandwidth and depriving the necessary room for designing a robust controller $C(\boldsymbol{s})$ which satisfies the practical requirements and constraints.

3.3 Eigenvalue Domain Analysis

The frequency domain analysis in the previous section indicated a notch characteristic of the lateral acceleration transfer functions $V_{CG}(\boldsymbol{s})$ at CG and $V_S(\boldsymbol{s})$ at sensor location S, with a natural mode around $0.5 - 2\,\mathrm{Hz}$. For increasing speed v, the phase lag associated with the natural mode increases due to $V_{CG}(0) \gg V_{CG}(\infty)$ in (13) and (14), and, for small look-ahead d_S, also for $V_S(0) \gg V_S(\infty)$ in (15) and (16). Furthermore, gain "undershoot" for $1 - 2\,\mathrm{Hz}$ hints a dominant and poorly damped zero-pair. The pole-zero locations of $V_{CG}(\boldsymbol{s})$ are studied in more detail in Fig. 9.

Observations

The left graph of Fig. 9 shows the dependency of pole and zero locations of $V_{CG}(\boldsymbol{s})$ on speed $10\,\mathrm{m/s} \leq v \leq 40\,\mathrm{m/s}$ on good road with $\mu = 1$. Poles follow circular arcs for speed variation while zeros follow parabolas. For increasing speed, both the poles and the zeros approach the imaginary axis, leading to respective poor damping, with the zeros having less damping than the associated pole-pair. Also, the pole and zero locations change significantly from $v = 10\,\mathrm{m/s}$ to $v \approx 25\,\mathrm{m/s}$, but vary less for increasing the speed further.

The dependendy of pole-zero locations of $V_{CG}(\boldsymbol{s})$ on $0.5 \leq \mu \leq 1$ for high speed $v = 40\,\mathrm{m/s}$ is depicted in the right graph of Fig. 9. Note the different scale of the real axis compared to

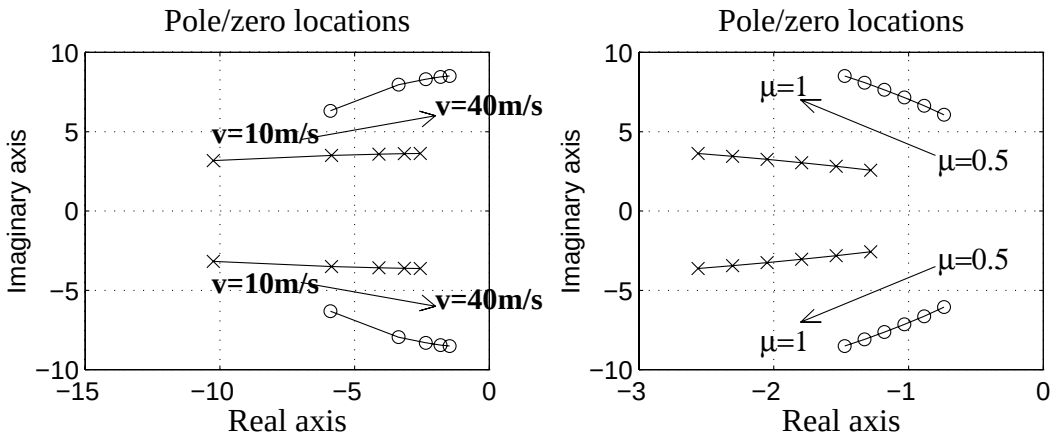

Fig. 9: Pole ('x') and Zero ('o') locations of $V_{CG}(\boldsymbol{s})$ for variation of speed $10\,\mathrm{m/s} \le v \le 40\,\mathrm{m/s}$ on good road with $\mu = 1$ (left graph) and variation of $0.5 \le \mu \le 1$ for high speed $v = 40\,\mathrm{m/s}$ (right graph)

the left graph. For decreasing μ, poles and zeros further approach the imaginary axis in a uniform manner. This results in even lower damping of both the pole-pair and the zero-pair.

The dominance of the zero-pair apparent in Fig. 9 is emphazised in Fig. 10. Damping D_p of the poles of $V_{CG}(\boldsymbol{s})$ (right graph) is contrasted with damping D_z of the zero-pair (left graph). Obviously, the numerator damping is significantly smaller than denominator damping. Even worse, damping D_z of the zeros decreases sharply with increasing speed to values as low as $D_z < 0.35$ for $v = 20\,\mathrm{m/s}$ and further to $D_z < 0.2$ for $v = 40\,\mathrm{m/s}$ on any road surface μ. Damping of the poles, on the other hand, drops steadily with speed to $D_p < 0.6$ at $v = 40\,\mathrm{m/s}$. Deteriorating road adhesion μ further decreases D_p for any speed, e.g. to $D_p < 0.45$ at $v = 40\,\mathrm{m/s}$ on wet road $\mu = 0.5$.

The yaw rate transfer function (4) shares denominator $\mathcal{D}(\boldsymbol{s})$ in (3) with lateral acceleration transfer function (6), but has only one (real) zero. (Yaw acceleration $W(\boldsymbol{s})$ in (4) has an additional zero in the origin.) Once again, addition of $V_{CG}(\boldsymbol{s})$ and $(d_S W(\boldsymbol{s}))$ to form $V_S(\boldsymbol{s})$ in (7) is nontrivial. Obviously, only the locations of the zeros change with varying d_S.

Damping associated with the zeros of the lateral acceleration transfer function $V_S(\boldsymbol{s})$ at sensor location S in (7) increases with look-ahead distance d_S, see Fig. 11 for an example at high speed $v = 40\,\mathrm{m/s}$ on a good road. The damping increase is dramatic for initial increases of d_S up to about twice the car length. For even larger d_S, the further damping increase is less significant. Equal damping of poles and zeros is achieved in the above example of Fig. 11 for $d_S \approx 15\,\mathrm{m}$.

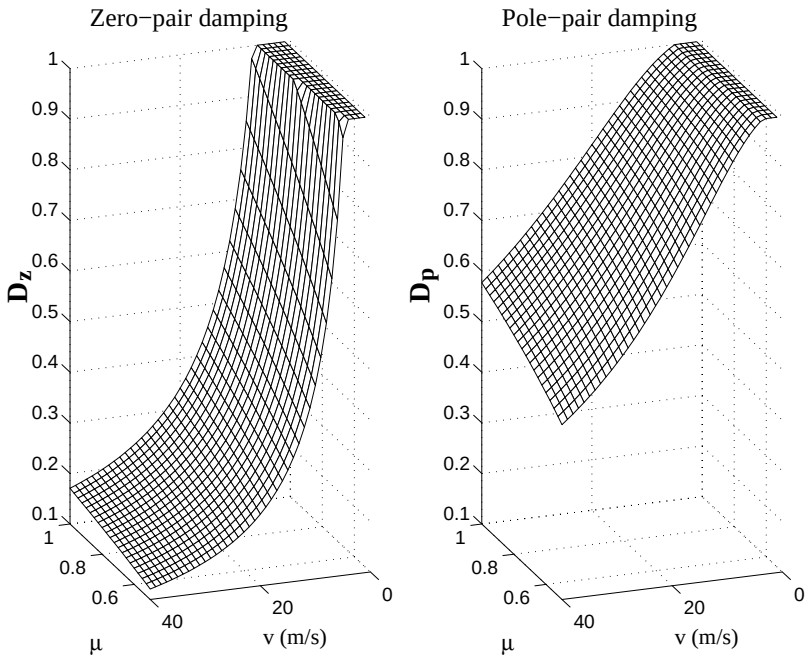

Fig. 10: Damping of the zero-pair (left) and the pole-pair (right) of the lateral acceleration transfer function $V_{CG}(\boldsymbol{s})$ for speed $1\,\mathrm{m/s} \leq v \leq 40\,\mathrm{m/s}$ and road adhesion $0.5 \leq \mu \leq 1$

Consequences for control

The locations of poles and zeros in the lateral acceleration transfer function $V_S(\boldsymbol{s})$ in (7) have significant consequences for control design for look-down systems with small d_S, especially at higher speeds. The degraded damping of the poles is a poor basis for control design to begin with, since $V_S(\boldsymbol{s})$ is a vital component of the overall 'control' $G(\boldsymbol{s})$ in (11) used to stabilize the double integrator plant. For closing the control loop, $C(\boldsymbol{s})$ requires one zero, better one zero-pair, in the left half plane to move the double integrator poles away from the origin. Simultaneously, the vehicle poles of $V_S(\boldsymbol{s})$ in (7) immediately start moving towards the imaginary axis when closing a feedback loop, leading to even poorer damping in closed loop $H(\boldsymbol{s})$ in (12) than in open loop $G(\boldsymbol{s})$ in (11). Furthermore, the zero-pair present in the lateral acceleration dynamics $V_S(\boldsymbol{s})$ with extremely poor damping for small d_S, attracts a pole-pair when closing the feedback loop. This leads to a poorly damped pole-pair in closed loop and outrules the use of high gain.

Hence, a second zero-pair is required to temporarily detract the vehicle poles in (3) away from the $\jmath\omega$-axis to improve damping. Introducing two zero-pairs in $C(\boldsymbol{s})$ amounts to strong differentiation action in the associated frequency ranges, since the controller poles need to be placed *away* from the zeros to avoid cancellation of their effects. Strong differentiation action in $C(\boldsymbol{s})$ leads to high gain at high frequencies, which amplifies high frequency noise and collides with actuator dynamics, as discussed in Section 3.2.

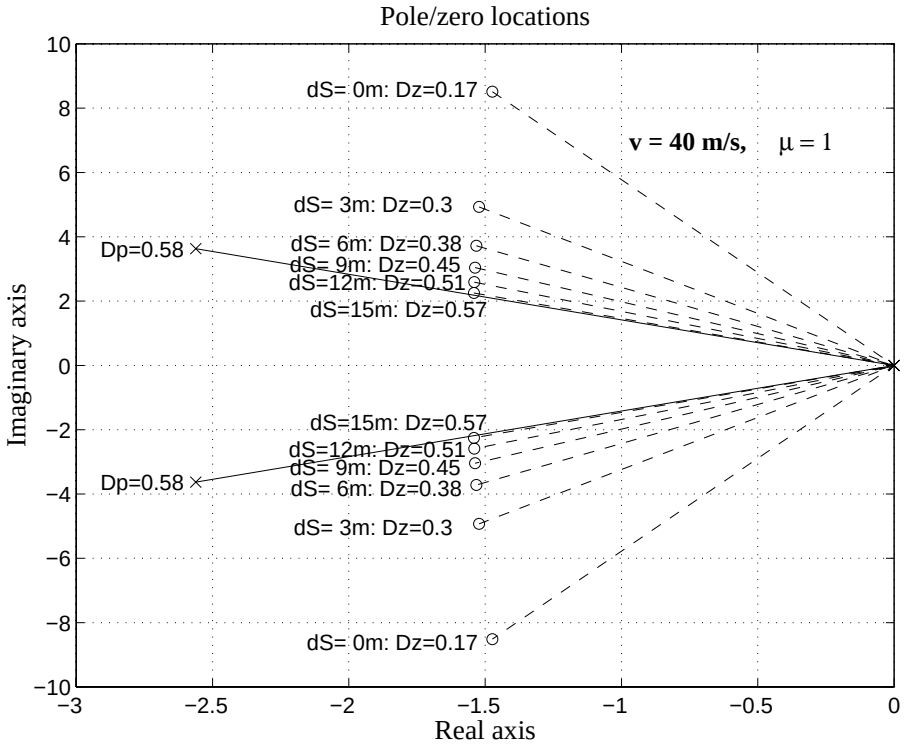

Fig. 11: Zero locations and associated damping for variation of look-ahead distance d_S for high speed $v = 40\,\mathrm{m/s}$ on good road with $\mu = 1$

An "almost" pole/zero cancellation could be achieved by moving a pole-pair close to the dominant zero-pair of the lateral acceleration dynamics at S via feedback. Besides the obvious concern of a poorly damped pole/zero cancellation, inacceptable comfort results. The closed loop poles are present in all vehicle transfer functions, i.e. in lateral accleration dynamics at all locations away from S and also in the yaw dynamics. However, only in the lateral acceleration transfer function $V_S(\boldsymbol{s})$ at sensor location S, the zero-pair present there would compensate the effect of poorly damped poles. In all other transfer functions, the poor damping surfaces uncompensated, leading to an effect called "fish-tailing": While sensor location S might exhibit acceptable tracking performance in closed loop, the vehicle itself yaw oscillates about S as if being hinged there. This effect also prevents utilisation of feedback linearization or inverse dynamics methods, which similarly would place controller poles close to poorly damped vehicle zeros. Furthermore, robustness requirements with respect to road adhesion μ raise serious doubts about the reliability of using pole-zero cancellation in the vicinity of the imaginary axis.

3.4 Physical Interpretation

The described vehicle dynamics and their dependence on speed v and road adhesion μ are best understood in a physical context. In the sequel, the dominant phenomena in the crucial lateral acceleration transfer functions $V_{CG}(\boldsymbol{s})$ and $V_S(\boldsymbol{s})$ will be studied: high frequency and steady state gain, and pole and zeros locations.

The *high frequency gain* of lateral acceleration transfer function at CG in (14) describes the instantaneous acceleration as a ratio of instantaneous force at the front tires for a step in steering angle δ_f, $(\mu c_f \delta_f)$, and the total vehicle mass M. At other locations away from CG, e.g. at d_S as in (16), a component of instantaneous yaw acceleration $\left(\mu c_f \frac{d_S \ell_f}{I_\Psi} \delta_f\right)$ is added. Linear proportioning of lateral force at the front tires with respect to the instantaneous angle between the front tire and the vehicle velocity vector $\mathbf{v}$ at the front axle is a result of the linear tire model used in this study. Hence, instantaneous acceleration is linear in road adhesion μ, but is speed independent.

Steady state lateral acceleration, on the other hand, derives from the force and torque balance equations, see e.g. [24, 26]. For neutral steer with $c_f \ell_f = c_r \ell_r$, (13) and (15) for any location d_S reduce to geometric cornering

$$\begin{aligned} \Big(V_{CG}\,(0)\Big)_{ns} &= V_{CG}\,(0)\Big|_{c_f \ell_f = c_r \ell_r} \\ &= \frac{v^2}{\ell}, \end{aligned} \tag{20}$$

with quadratic speed dependence according to centrifugal force equilibria. Understeer with $c_f \ell_f < c_r \ell_r$ is generated in all passenger cars by locating the CG ahead of the mid-point between the two axles. This reduces the sensitivity of the vehicle at higher speed by creating a torque opposing the geometric cornering (20). In effect, the gain from steering angle to lateral acceleration is decreased below $\frac{v^2}{\ell}$, resulting in a v^κ, $(1 < \kappa < 2)$ dependency of $V_{CG}(0)$ in (13) at moderate speed and even a $(0 < \kappa < 1)$ dependency at very high speeds. The benefit for human driving is desensitization of the steering at higher speed. In other words, to drive a specified radius of curvature, a larger steering angle is required at high speed than at low speed. Due to the remaining v^κ dependency, however, a steady state gain lower than the speed independent high frequency gain at low speed turns into a steady state gain $V_{CG}(0)$ greater than $V_{CG}(\infty)$ at higher speeds, with associated phase lag instead of phase lead.

Pole locations derive from the dynamic motion equations of the lateral and the yawing modes. For neutral steer, the poles in (3),

$$\begin{aligned} \Big(\mathcal{D}(\boldsymbol{s})\Big)_{ns} &= \mathcal{D}(\boldsymbol{s})\,\Big|_{c_f \ell_f = c_r \ell_r} \\ &= \left(\boldsymbol{s} + \mu \frac{c_f + c_r}{M v}\right)\left(\boldsymbol{s} + \mu \frac{c_f \ell_f^2 + c_r \ell_r^2}{I_\Psi v}\right), \end{aligned} \tag{21}$$

are real and clearly separated into the lateral (translational) mode and the yawing (rotational) mode. For example, the yaw rate transfer function (4) reduces to the first order yawing mode (right factor in (21)), since the lateral mode (left factor in (21)) appears as a zero for neutral steer $c_f\ell_f = c_r\ell_r$. Note that both modes linearly depend on road ahesion μ and on the inverse of speed v, in compliance with basic motion laws.

Understeer introduces coupling between the lateral and the yawing modes. For decreasing the overall steady state gain both in $V_{CG}(\boldsymbol{s})$ and $V_S(\boldsymbol{s})$, the understeer term $\frac{\mu}{I_\Psi}(c_f\ell_f - c_r\ell_r) < 0$ in denominator $\mathcal{D}(\boldsymbol{s})$ in (3) increases the natural frequency ω_p of the poles when written as

$$\mathcal{D}(\boldsymbol{s})(\boldsymbol{s}) \;=\; I_\Psi M v^2(\boldsymbol{s}^2 + 2D_p\omega_p\boldsymbol{s} + \omega_p^2). \tag{22}$$

Increasing ω_p for constant $(2D_p\omega_p)$ decreases damping D_p and eventually leads to a complex pole pair. Since understeer at higher speed creates a torque opposing the geometric cornering, the front tires have to support more lateral forces than the rear tires. Due to the shorter lever arm of the front tires compared to the rear tires for any $d_S > 0$, understeer results in decreased total lateral damping forces provided by the tires.

The *zeros* of a mechanical system are tightly connected to input and output locations. In particular, a zero in a transfer function signifies that an energy injection with the zero frequency at the input is absorbed by the system and will not (fully) reach the output. Conversely, a disturbance at the output with zero frequency does not show (much) effect at the input location. This implies that the modes of the system obtained by mechanically constraining an input constitute the overall system zeros for that input.

For the lateral vehicle dynamics, mechanically constraining the front tires, i.e. "hinging" the vehicle at the front axle, describes the zeros of the lateral transfer functions for any d_S as the poles of the hinged system. Consequently, the zeros are comprised of a translational mode coupled with a rotational mode about a vertical axis at the front axle and thus do not depend on front tire characteristics like stiffness c_f. Also, damping of the hinged system is only provided by lateral damping of the rear tires. Hence for small d_S, the zeros in the lateral acceleration transfer function in (7) have less damping than the vehicle poles, which can draw upon damping from all four tires. The smaller zero damping compared to the pole damping is most noticable for higher speed, when lateral damping from the tires becomes more critical.

Understanding the zeros of $V_S(\boldsymbol{s})$ in (7) as the modes of the vehicle being hinged at the front axle also explains the influence of look-ahead distance d_S on damping of those zeros: The larger the lever arm $(d_S - \ell_f)$ to the front axle compared to the rear lever arm $\ell = \ell_f + \ell_r$, the better the damping of the zeros. Initial increases of absolute d_S out from the front bumper have a larger impact on the lever arm ratio and hence on the damping of the zeros than for large look-ahead $(d_S - \ell_f) > \ell$, as already observed in Section 3.3.

4 Control Design Directions

This section is devoted to an investigation of possible control design directions. Since this paper concentrates on fundamental issues in automatic steering control, no explicit control design is discussed here. Rather, basic design directions are examined and contrasted with respect to their advantages and possible drawbacks, emphasizing on the performance requirements and practical constraints discussed in Sections 2.2 and 2.3.

The analysis in Section 3.3 indicates that the zero-pair of the lateral acceleration transfer function $V_S(\boldsymbol{s})$ in (7) is one of the major obstacles towards automatic steering control design for look-down reference systems with small look-ahead d_S. Recall that the zero-pair has extremely poor damping for higher speed, e.g. less than 0.2 damping for $v \geq 40\,\mathrm{m/s}$ on any road surface. In a closed loop system, a pole-pair is inevitably attracted to the zero-pair, leading to low pole damping. Since these poles dominate other vehicle transfer functions like lateral acceleration away from sensor location S and vehicle yaw rate, poor comfort results. Feedback of additional internal states like vehicle yaw rate cannot solve this problem of attractive, but poorly damped zeros, since only pole locations can be influenced.

The necessary modification of zero locations requires changing the overall plant structure as outlined in Section 3.4. In general, two alternatives exist: modifying the inputs or modifying the outputs of the system.

For changing the plant input(s), various methods of generating a lateral force or a yaw torque acting on the vehicle can be exploited [29]. Prominent examples include single-wheel braking as being used for Anti-Skid-Control (ASC) by Mercedes-Benz and Bosch in Germany [30] and the robust yaw decoupling control for four-wheel steered (4WS) cars [31]. ASC generates a yaw torque to avoid skidding in emergency situations by braking of selected wheels and thus can hardly be used in continuous operation for automatic steering. An appropriate equivalent would be single wheel driving torques on all four wheels, a technically rather involved and expensive solution.

The 4WS control law by Ackermann [31], on the other hand, is suited for continuous AHS operation at the price of an additional rear wheel steering mechanism. Robust decoupling of yaw motion from lateral acceleration at the front axle is achieved by feedback of the vehicle yaw rate via an integrator. The control law exploits structural properties of the vehicle dynamics and is robust with respect to parameters like car mass and inertia, road condition, and even nonlinear tire characteristics.

The approaches mentioned above aim at modifying the inputs to the lateral vehicle dynamics and thus require expensive changes to the mechanical structure of the car. In the discussion below, we will focus on a less involved solution, the modification of the system outputs to influence the location of the zeros of the lateral acceleration transfer function for automatic steering control.

4.1 Modification of look-ahead: The dual roles concept

The new problem description in Fig. 3, with open loop $G(\boldsymbol{s})$ in (11) and closed loop $H(\boldsymbol{s})$ in (12), reveals an interesting phenomenon. Plant $\left(\frac{1}{\boldsymbol{s}^2}\right)$ in (9), the double integrator from lateral acceleration error $\Delta\ddot{y}_S$ to lateral displacement Δy_S, is controlled by $G(\boldsymbol{s}) = A(\boldsymbol{s})V_S(\boldsymbol{s})C(\boldsymbol{s})$ where $C(\boldsymbol{s})$ comprises the controller, $V_S(\boldsymbol{s})$ represents the vehicle lateral dynamics at S and $A(\boldsymbol{s})$ denotes the actuator dynamics. Instead of isolated design of controller $C(\boldsymbol{s})$, the vehicle dynamics $V_S(\boldsymbol{s})$ are now included in the design of $G(\boldsymbol{s})$ to control the double integrator. In fact, for practical implementation, also actuator dynamics $A(\boldsymbol{s})$ have to be taken into account, although it might not be possible to modify them significantly for a given car.

A set of new design directions evolves from this novel point of view. First, an appropriate $G(\boldsymbol{s})$ is designed, taking in account all practical requirements and constraints on closed loop $H(\boldsymbol{s})$. Then, $G(\boldsymbol{s})$ is realized via concurrent design of vehicle dynamics $V_S(\boldsymbol{s})$ and controller $C(\boldsymbol{s})$. In this second step, $V_S(\boldsymbol{s})$ and $C(\boldsymbol{s})$ play complementary roles and may be regarded dual to each other.

Plant $\left(\frac{1}{\boldsymbol{s}^2}\right)$ in (9) is known exactly. Combined "controller" $G(\boldsymbol{s})$ should be designed for closed-loop $H(\boldsymbol{s})$ to fulfill the performance requirements discussed in Section 2.2, in particular with respect to maximum lateral displacement, damping for ride comfort, and robustness with respect to road adhesion μ. Furthermore, zero steady-state errors and controller roll-off to prevent exciation of actuator dynamics are required. Reference acceleration $\ddot{y}_{\text{ref}}$ can be known from (9) via appropriate transmission of preview information of up-coming curvature from the road to the vehicle. For example, in the magnetic marker system used at California PATH, binary coding of magnet polarity is used to preview road curvature before encountering a road curvature change [19, 32]. In case of availability of preview, feed-forward of road curvature can be added to the overall control structure, but is subject to dynamic uncertainty. Since curvature preview does not significantly influence stability, this option is not persued in the sequel.

The double integrator (9) has to be stabilized by $G(\boldsymbol{s})$ via a lead compensator with approximately 60^o phase lead at cross-over for appropriate damping. At low frequencies, below roll-off, a minimum gain according to (17) is necesssary to achieve the performance requirements. Also, $G(\boldsymbol{s})$ needs to include integral action for zero steady state lateral displacement and low-pass characteristics for the desired roll-off.

The simplest linear solution is a PID_mT_n structure for $G(\boldsymbol{s})$, where the proportional gain P is determined to satisfy (17), the integral I-term is chosen not to interfer with stability, i.e. does not introduce phase lag in the vicinity of cross-over, the differential term D_m is an m-th order lead compensator to provide sufficient phase margin, and T_n is an n-th order low pass for roll-off with $n > m$. This PID_mT_n structure is synthesized by design of lateral

vehicle dynamics $V_S(\boldsymbol{s})$ and controller $C(\boldsymbol{s})$ to form $G(\boldsymbol{s})$ in (11). Actuator dynamics $A(\boldsymbol{s})$ in (8) are not included in the design, however, bandwidth and damping requirements for the position control of the actuator derive from the requirements on $G(\boldsymbol{s})$.

Lateral acceleration $V_S(\boldsymbol{s})$ at S has second order dynamics with two poles and two zeros. Depending on speed v, road adhesion μ and look-ahead distance d_S with fixed parameters of the vehicle dynamics (e.g. as in Table 1), $V_S(\boldsymbol{s})$ shows charactersistics of either a lead compensator or a lag compensator, see also Fig. 7. In particular, at low speed, e.g. for $v = 10\,\mathrm{m/s}$, small look-ahead d_S already provides substantial phase lead for the full range of considered road adhesion $0.5 \leq \mu \leq 1$. For higher speeds, small d_S as present in look-down reference systems, results in phase lag, e.g. up to 70^o on poor road surface at $v = 40\,\mathrm{m/s}$. Increasing look-ahead d_S reverses this trend. For example, for

$$d_{S0} \;=\; \frac{I_\Psi/M\,(v^2\mu(c_f+c_r)\ell_f - \mu^2 c_f c_r \ell^2)}{\ell_f\,(Mv^2\mu(c_r\ell_r - c_f\ell_f) + \mu^2 c_f c_r \ell)} \tag{23}$$

$V_S(0) = V_S(\infty)$ and hence the overall phase balance is equal to zero. Furthermore, phase lead is present in $V_S(\boldsymbol{s})$ for sufficiently large $d_S > d_{S0}$ in the frequency range of the natural mode.

In addition to vehicle dynamics $V_S(\boldsymbol{s})$, controller $C(\boldsymbol{s})$ may also provide phase lead for stabilization. The interchangeability of the roles of $V_S(\boldsymbol{s})$ and $C(\boldsymbol{s})$ in $G(\boldsymbol{s})$ to stabilize the double integrator plant (9) with sufficient phase margin is the core of the ***dual roles concept***.

Case I: Look-ahead distance d_S is chosen such that $V_S(\boldsymbol{s})$ contributes sufficient phase lead to $G(\boldsymbol{s})$ for stabilization of $(1/\boldsymbol{s}^2)$ for the range $0.5 \leq \mu \leq 1$. Controller $C(\boldsymbol{s})$ is chosen with PI-type characteristics to match the phase lead region of $V_S(\boldsymbol{s})$ with the cross-over region for plant (9). The special case of *Hurwitz* stability for a good road surface was solved for a true look-ahead system by Ünyelioğlu *et al.* [13].

Case II: Look-ahead distance d_S is chosen similar to (23) such that $V_S(\boldsymbol{s})$ contributes no or little overall phase lag/lead to $G(\boldsymbol{s})$ and is approximately a P-type transfer function for the range $0.5 \leq \mu \leq 1$. Controller $C(\boldsymbol{s})$ is chosen with a $\mathrm{PID}_m\mathrm{T}_n$ characteristic to provide sufficient phase lead to $G(\boldsymbol{s})$ for stabilization of $(1/\boldsymbol{s}^2)$, according to the performance requirements.

Intermediate solutions include sharing phase lead requirements between $V_S(\boldsymbol{s})$ and $C(\boldsymbol{s})$, and compensating phase lag in $V_S(\boldsymbol{s})$ by $C(\boldsymbol{s})$ or visa versa. Note that compensation of phase lag in $V_S(\boldsymbol{s})$ requires strong differentiating action of $C(\boldsymbol{s})$ which may collide with noise and actuator constraints. For studying the respective merits of the different approaches, contrast the two cases on an abstract level. The main differences are:

- Case I requires larger look-ahead distances d_S than case II, which generally leads to a higher noise level in the lateral displacement measurement Δy_S.
- Case II requires more phase lead of controller $C(\boldsymbol{s})$ than case I, leading to higher controller gain in the mid-frequency range, around and after cross-over, which generally amplifies higher frequency noise.
- For case I, cross-over is determined by the phase lead region of $V_S(\boldsymbol{s})$. Since cross-over and hence closed-loop bandwidth is confined to a range prescribed by the vehicle dynamics, the P-portion of controller $C(\boldsymbol{s})$ cannot be chosen to satisfy arbitrary performance requirements. However, it turns out that the performance requirements are almost satisfied for most passenger cars. Variation of road adhesion μ simultaneously influences the low frequency gain of $V_S(\boldsymbol{s})$ and frequency range of phase lead such that simultaneous stabilization of $(1/\boldsymbol{s}^2)$ in (9) is possible, see the left Bode diagram in Fig. 12 for an example for $v = 40\,\mathrm{m/s}$, $d_S = 16.9\,\mathrm{m}$ (resulting in a minimum phase lead of 50^o), $\mu_1 = 1$ and $\mu_2 = 0.5$, with P-control $C(\boldsymbol{s}) = 0.03$. Inherent "almost" satisfaction of performance requirements and robustness with respect to road adhesion are attributed to the specifications of vehicle steering design to accomodate human driving behavior. In fact, it can be argued that case I resembles the steering characteristics of a concentrated human driver.
- For case II, cross-over is determined entirely by control $C(\boldsymbol{s})$ and can be chosen to satisfy any performance requirements. Since $C(\boldsymbol{s})$ is invariant with respect to road adhesion (adaptation is not possible since μ is not slowly time-variant), robustness is to be achieved by providing phase lead over a range of possible cross-over frequencies, see the right Bode diagram of Fig. 12. The example shows a similar situation as above, with $d_S = 5.8\,\mathrm{m}$ and $C(\boldsymbol{s}) = 0.03L(50)$, where $L(50)$ denotes a higher order lead compensator, providing 50^o phase lead consistently over the necessary frequency range.

The above list points out the crucial trade-offs in automatic steering control design. Noise in lateral displacement measurement Δy_S increases at least linearly in d_S for sensors "looking ahead" of the front bumper, and even quadratically in d_S e.g. for maschine vision. On the other hand, poviding phase lead in $C(\boldsymbol{s})$ leads to higher controller gain at higher frequencies around and after cross-over, which may require excessive actuator bandwidth. These noise considerations have to be traded off with the ability to satisfy performance requirements. Case I, using "natural" phase lead in $V_S(\boldsymbol{s})$ by appropriate seletion of d_S offers straight forward control design at the price of a pre-determined cross-over frequency and hence pre-determined system bandwidth. Only two control parameters, d_S and the P-gain, have to be selected for robustness with respect to the range $0.5 \leq \mu \leq 1$, possibly gain-scheduled with velocity v. Case II, on the other hand, provides flexibility in choosing cross-over, but requires more involved, higher order control design. For example, the plain 50^o-phase lead controller $L(50)$ shown in Fig. 12 is not directly employable due to corruption by the vehicle dynamics $V_S(\boldsymbol{s})$ as apparent from the right Bode diagram.

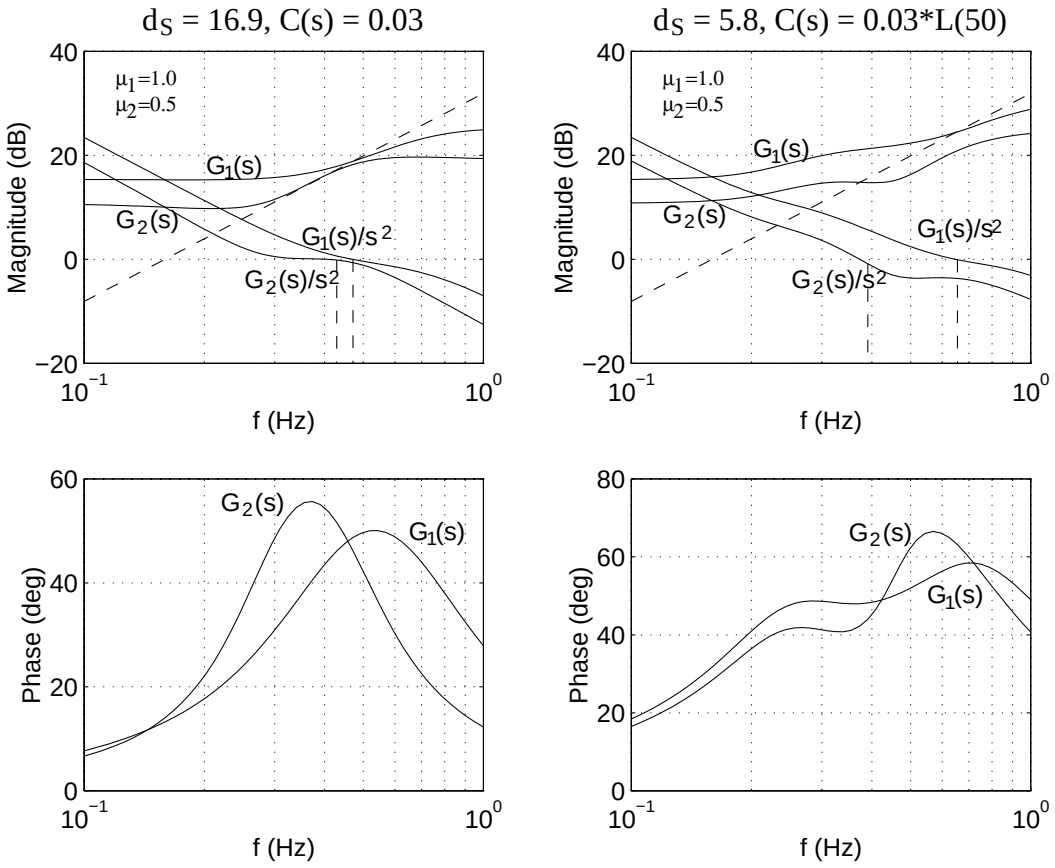

Fig. 12: ***Dual roles concept*** **:** Robust stabilization by vehicle phase lead with long look-ahead d_S (Case I, left Bode diagram) is dual to robust stabilization by a lead compensator with small look-ahead d_S (Case II, right Bode diagram)

4.2 Virtual look-ahead

In addition to the obvious solution of employing true look-ahead reference systems like machine vision [7–12] or radar [13], vitual look-ahead can be created for look-down reference systems to virtually extend d_S beyond the front bumper. Look-down reference systems are attractive with respect to reliability and accuracy, e.g. magnetic markers [19] are not susceptible to weather and light conditions like machine vision and the sensor field of view may not be obstructed by preceeding vehicles, which is important for platooning [6]. To preserve the advantages of look-down reference systems via virtual look-ahead, consider equation (7), which can be re-written in error coordinates for virtual look-ahead d_v as

$$\begin{aligned} \Delta\ddot{y}_v &= (\ddot{y}_{CG} - v^2\rho_{\text{ref}}) + d_v(\ddot{\Psi} - v\dot{\rho}_{\text{ref}}) \\ &= \Delta\ddot{y}_{CG} + d_v\Delta\ddot{\Psi}. \end{aligned} \tag{24}$$

Note that $\dot{\rho}_{\text{ref}}$ is a *Dirac* impulse for step changes of road curvature. However, (24) is written in terms of acceleration, which is the control variable, but not the measured variable. Measurements are on position scale (e.g. Δy_{CG}) or, at best, on velocity scale (e.g. $\dot{\Psi}$).

It is clear from (24) that a virtual look-ahead $d_v > d_S$ requires measurement of $\Delta\Psi$ or $\Delta\dot{\Psi}$, e.g. by

Method I: Measurement of yaw rate $\dot{\Psi}$, speed v and preview of road curvature ρ_{ref} to obtain the rate of angular displacement,

$$\Delta\dot{\Psi} = \dot{\Psi} - v\rho_{\text{ref}}. \tag{25}$$

Method II: Measurement of lateral displacement Δy_T at a location near the tail of the vehicle (see Fig. 13) to obtain angular displacement $\Delta\Psi$ as

$$\Delta\Psi \;=\; \frac{\Delta y_S - \Delta y_T}{d_S + d_T}. \tag{26}$$

Method III: Combination of methods I and II in a *Kalman* filter structure.

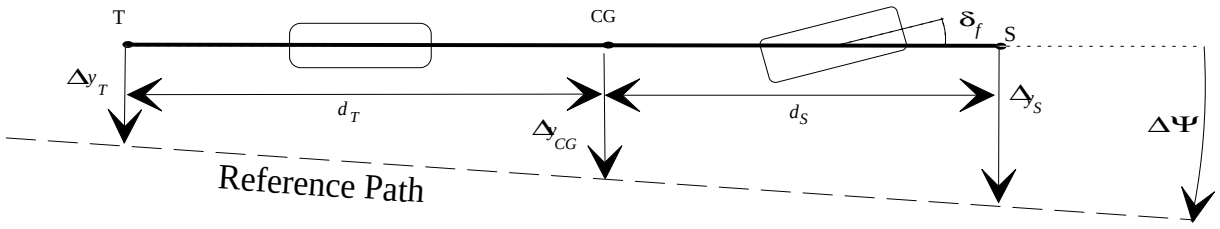

Fig. 13: Using an additional lateral displacement sensor T at the tail of the vehicle to measure the angular displacement $\Delta\Psi$

Method I has the advantage of providing a velocity scale measurement ($\Delta\dot{\Psi}$) as compared to a position scale measurement ($\Delta\Psi$) of method II. Since, at least for controller case II, differentiating action is required of controller $C(\boldsymbol{s})$, measurement of an already differentiated variable $\Delta\dot{\Psi}$ is attractive. However, the difference of two absolute variables $\dot{\Psi}$ and $v\rho_{\text{ref}}$ is used to calculate relative variable $\Delta\dot{\Psi}$, with obvious noise concerns. On the other hand, method II calculates relative variable $\Delta\Psi$ via two relative measurements Δy_S and Δy_T. The effect of measurement noise determines the respective practical merits of the two methods, but is too implementation specific to be studied in a general setting. Obviously, method III

combines the advantages of methods I and II, and has a potential to trade off their disadvantages, i.e. support differentiating action to get phase lead in the presence of measurement noise.

In contrast to reference systems with true look-ahead, the above methods enable utilization of frequency functions for look-ahead distance, e.g. a virtual look-ahead $d_v(\boldsymbol{s})$ can be defined for a virtual displacement measurement

$$\Delta y_v(\boldsymbol{s}) \;=\; \Delta y_{CG} + d_v(\boldsymbol{s})\Delta\Psi, \tag{27}$$

to obtain a steering controller of the form

$$\begin{aligned} \delta &= C(\boldsymbol{s})\Delta y_v(\boldsymbol{s}) \\ &= C_{CG}(\boldsymbol{s})\Delta y_{CG} + C_\Psi(\boldsymbol{s})\Delta\Psi. \end{aligned} \tag{28}$$

Virtual look-ahead $d_v(\boldsymbol{s}) = \frac{C_\Psi(\boldsymbol{s})}{C_{CG}(\boldsymbol{s})}$ allows to select a frequency range of measurement $\Delta\Psi$, e.g. to accomodate the *Kalman* filter structure of method III and for bandpass filtering to obtain the necessary phase lead in the $0.1 - 2\,\mathrm{Hz}$ region to compensate phase lag introduced by $V_{CG}(\boldsymbol{s})$.

For implementation with a tail displacement sensor T as depicted in Fig. 13, (28) can be re-written as

$$\delta \;=\; C_S(\boldsymbol{s})\Delta y_S + C_T(\boldsymbol{s})\Delta y_T, \tag{29}$$

with $C_S(\boldsymbol{s}) = \dfrac{d_T C_{CG}(\boldsymbol{s}) + C_\Psi(\boldsymbol{s})}{d_S + d_T}$ and $C_T(\boldsymbol{s}) = \dfrac{d_S C_{CG}(\boldsymbol{s}) - C_\Psi(\boldsymbol{s})}{d_S + d_T}$.

4.3 Modification of system zeros

Virtual look-ahead, i.e. $d_v(\boldsymbol{s})$ in (27), allows to modify the system zeros. We have argued that the poor damping of the zero pair in the lateral acceleration transfer function (7) at high speeds substantially hinders automatic steering control design for look-down reference systems under practical conditions, see also [22]. Furthermore, cancellation of the zeros by moving the system poles into their vicinity via feedback is inadequate because the poles in (3) are also present in all other vehicle transfer functions like yaw rate (4) and poor pole damping would result.

The capability to influence the system zeros via virtual look-ahead, however, provides means to achieve pole-zero compensation by moving the zeros close to the poles instead, preserving the original pole locations. Consider Fig. 14 with an example of method II at $v = 40\,\mathrm{m/s}$, with $\mu = 0.5$ in the left graph and $\mu = 1$ in the right graph. The modification of zero ('o') locations is illustrated for variation of gain K_T in virtual lateral acceleration

$$V_v(\boldsymbol{s}) \;=\; \frac{1}{T_S\boldsymbol{s}+1}V_S(\boldsymbol{s}) - \frac{K_T}{T_T\boldsymbol{s}+1}V_T(\boldsymbol{s}), \tag{30}$$

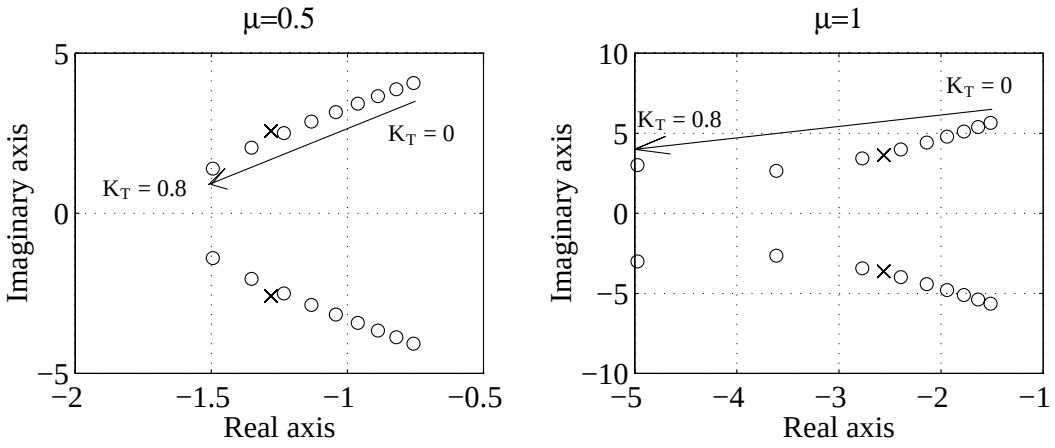

Fig. 14: Modification of zeros ('o') in virtual lateral acceleration transfer function $V_v(\boldsymbol{s})$ in (30) with gain K_T to compensate the poles ('x') in $\mathcal{D}(\boldsymbol{s})$ (3)

with $T_S > T_T$ and $V_T(\boldsymbol{s})$ denoting the lateral acceleration transfer function for $\ddot{y}_T$ at the tail sensor T.

For appropriate $K_T(v)$, gain scheduled with speed v, the zeros ('o') are within the close vicinity of the poles ('x') for the full range of $0.5 \leq \mu \leq 1$ and $V_v(\boldsymbol{s})$ turns into a PT_1 transfer function, already providing the roll-off necessary for noise attenuation. Henceforth, controller $C(\boldsymbol{s})$ can be designed independently to stabilize the double integrator plant $(1/\boldsymbol{s}^2)$ according to the performance requirements of Section 2.2, considering only the gain variation in $V_v(0)$ with respect to road adhesion and velocity. The 50^o phase lead controller $L(50)$ introduced in the right Bode diagram of Fig. 12 now is adequate, since $G(\boldsymbol{s})$ is not corrupted by the vehicle dynamics as previously with plain increase of look-ahead to $d_S = 5.8\,\mathrm{m}$. Also, since the vehicle pole-pair is not altered in (30) and the vehicle zero-pair is placed in its vicinity, vehicle damping and hence ride comfort is guaranteed to be similar as in the conventional, manually steered car.

5 Conclusions

This paper discussed fundamental issues in lateral control design for automatic steering of passenger cars within an Automated Highway System (AHS). Previous research over more than two decades employed a variety of reference systems to determine the lateral vehicle displacement from the road center. Reference systems can be categorized into look-down and look-ahead systems, depending on the point of displacement measurement with respect to the vehicle's center of gravity. Among the successful experimental implementations of both types of reference systems, look-down systems seem to have faced limitations in driving speed, independent of the control design. In an effort to understand the impacts of higher

driving speed under practical constraints and limitations of an AHS, a detailed analysis was presented using time and frequency domain tools together with physical insight into the vehicle dynamics. Performance requirements and system constraints such as maximum errors in the response to a step in road curvature, robustness with respect to abruptly changing road adhesion, ride comfort, measurement noise, and steering actuation considerations were directly included in the analysis.

The analysis revealed a dramatic change of the relevant lateral vehicle dynamics of look-down system for increasing speed. In particular, pole and zero locations vary such that damping decreases, for zeros even more than for the poles. Furthermore, instead of providing phase lead as for low speed, the lateral vehicle dynamics of look-down systems introduce significant phase lag for higher speed, preventing control design entirely based on feedback of the lateral displacement measurement. Look-ahead systems, on the other hand, provide sufficient phase lead even for higher driving speeds by adequately increasing the look-ahead distance. The respective influence of phase lead from lateral vehicle dynamics and look-ahead distance led to the formulation of a *dual roles concept* between the feedback controller and the vehicle dynamics in general automatic steering control design.

Several design directions were investigated, both for look-down and look-ahead systems. In order to preserve the qualities of look-down systems like reliability and accuracy, the concept of 'virtual look-ahead' via additional yaw error and yaw rate error measurements was introduced. Effectively, virtual look-ahead modifies the system zeros and remedies the speed limitations of look-down systems for lateral control design. A general framework was established for automatic steering control design based on the detailed analysis in the first part of the paper.

We conclude that proportional-type feedback design sufficies if the lateral vehicle dynamics itself provide phase lead for stabilization, which is the case for look-ahead systems. On the other hand, a phase lead controller is required for shorter look-ahead distances. The methodology of virtual look-ahead for look-down systems and its benefits for control design were illustrated using examples at $v = 40\,\mathrm{m/s}$. Subsequent work is under way to investigate explicit control designs and their respective benefits, concentrating on the utilization of physical system insight for feedback control. A number of control design approaches along the design directions presented in this paper are currently being validated in experiments at California PATH.

Acknowledgements

This work is performed as part of the *Partners for Advanced Transit and Highways* (PATH) program, prepared under the sponsorship of the State of California; Business, Transportation and Housing Agency; Department of Transportation (CalTrans).

We would like to express our sincere thanks to S. Shladover and W.-B. Zhang of California PATH, M. Tomizuka and K. Hedrick of the University of California at Berkeley, J. Ackermann, W. Sienel and T. Bünte of DLR (Germany), and K. Åström of Lund University (Sweden) for their insightful comments and suggestions.

References

[1] W. Stevens, "The automated highway system program: A progress report", in *Preprints of the 13th IFAC World Congress (plenary volume)*, San Francisco, CA, USA, 1996, pp. 25–34.

[2] Lateral and Longitudinal Control Systems Working Group, "Overview of the R&D and test on automated highway systems (AHS)", in *Intelligent Transport Systems*, Tsukuba, Japan, November 1995.

[3] S. Tsugawa, M. Aoki, A. Hosaka, and K. Seki, "A survey of present IVHS activities in Japan", in *Preprints of the 13th IFAC World Congress, Vol. Q*, San Francisco, CA, USA, 1996, pp. 147–152.

[4] J. G. Bender, "An overview of systems studies of automated highway systems", *IEEE Trans. on Vehicular Technology*, vol. 40, no. 1, pp. 82–99, 1991.

[5] S.E. Shladover, "Review of the state of development of advanced vehicle control systems (AVCS)", *Vehicle System Dynamics*, vol. 24, pp. 551–595, 1995.

[6] P. Varaiya, "Smart cars on smart roads: Problems of control", *IEEE Trans. on Automatic Control*, vol. 38, pp. 195–207, 1993.

[7] M. Maurer *et al.*, "VaMoRs-P: An advanced platform for visual autonomous road vehicle guidance", in *Proc. SPIE Conf. 'Mobile Robots IX'*, Boston, 1994.

[8] B. Ulmer, "VITA - An autonomous road vehicle (ARV) for collision avoidance in traffic", in *Proc. of Intelligent vehicles '92*, Detroit, 1992, pp. 36–41.

[9] B. Ulmer, "VITA II - Active collision avoidance in real traffic", in *Proc. of Intelligent vehicles '94*, Paris, 1994, pp. 1–6.

[10] H. Fritz, "Autonomous lateral road vehicle guidance using neural network controllers", in *ECC*, Rome, 1995, pp. 285–290 (Vol. 3).

[11] T. Jochem, D. Pomerleau, B. Kumar, and J. Armstrong, "PANS: A portable navigation platform", in *Proc. Intelligent vehicles Symposium*, Detroit, MI, USA, 1995, pp. 107–112.

[12] Q.-T. Luong, J. Weber, D. Koller, and J. Malik, "An integrated stereo-based approach to automatic vehicle guidance", in *Proc. of the 5th ICCV*, June 1995.

[13] K. A. Ünyelioğlu, C. Hatipoğlu, and Ü. Özgüner, "Design and stability analysis of a lane following controller", *IEEE Trans. on Control Systems Technology*, to appear in 1996.

[14] F. Andrew and M. Nakamura, "Lasar radar for a vehicle lateral guidance system", *US Patent no. 592235*, pp. 1–32, Oct. 3 1990.

[15] D. Margolis and Y. Yasui, "Automatic lateral guidance control system", *US Patent no. 5390119*, pp. 1–18, Feb. 14, 1995.

[16] R. E. Fenton, G. C. Melocik, and K. W. Olson, "On the steering of automated vehicles: Theory and experiment", *IEEE Trans. on Automatic Control*, vol. 21, no. 3, pp. 306–315, 1976.

[17] W. Darenberg, "Automatische Spurführung von Kraftfahrzeugen (in German)", *Automobil-Industrie*, pp. 155–159, 1987.

[18] R. J. Mayhan and R. A. Bishel, "A two-frequency radar for vehicle automatic control", *IEEE Trans. on Vehicular Technology*, vol. 31, no. 1, 1982.

[19] W. Zhang and R. E. Parsons, "An intelligent roadway reference system for vehicle lateral guidance/control", in *Proc. American Control Conf.*, San Diego, CA, USA, 1990, pp. 281–286.

[20] S.E. Shladover, "The California PATH program and its approach to vehicle-highway automation", in *Proc. Intelligent Vehicles Symp.*, Detroit, 1992, pp. 347–352.

[21] R. E. Fenton and R. J. Mayhan, "Automated highway studies at the Ohio State University - An overview", *IEEE Trans. on Vehicular Technology*, vol. 40, no. 1, pp. 100–113, 1991.

[22] J. Guldner, H.-S. Tan, and S. Patwardhan, "Analysis of automatic steering control for highway vehicles with look-down lateral reference systems", *Vehicle System Dynamics*, vol. 26, no. 4, pp. 243–269, 1996.

[23] S. E. Shladover *et al.*, "Automatic vehicle control developments in the PATH Program", *IEEE Trans. on Vehicular Technology*, vol. 40, no. 1, pp. 114–130, 1991.

[24] H. Peng and M. Tomizuka, "Vehicle lateral control for highway automation", in *Proc. American Control Conf.*, San Diego, CA, USA, 1990, pp. 788–794.

[25] P. Riekert and T.E. Schunck, "Zur Fahrmechanik des gummibereiften Kraftfahrzeugs (in German)", *Ingenieur Archiv*, vol. 11, pp. 210–224, 1940.

[26] J. Ackermann, A. Bartlett, D. Kaesbauer, W. Sienel, and R. Steinhauser, *Robust control: Systems with uncertain physical parameters*, Springer, London, 1993.

[27] H. Peng, W.-B. Zhang, S.E. Shladover, M. Tomizuka, and A. Arai, "Magnetic-marker-based lane keeping: A robustness experimental study", in *Proc. SAE Congress, SAE paper no. 930556*, Detroit, MI, USA, 1993, pp. 127–132.

[28] S. Patwardhan, M. Tomizuka, W.-B. Zhang, and P. Devlin, "Theory and experiments of tire blow-out effects and hazard reduction control for automated vehicle lateral control system", in *Proc. Int. Symp. on Advanced Vehicle Control*, Japan, 1994, pp. 426–431.

[29] K. A. Ünyelioğlu, Ü. Özgüner, J. Winkelman, and T. Hissong, "Nonstandard control inputs in the integrated design of vehicles", in *Proc. American Control Conf.*, Baltimore, 1994, pp. 816–820.

[30] A. v. Zanten, R. Erhardt, and G. Pfaff, "FDR - Die Fahrdynamikregelung von Bosch (in German)", *Automobiltechnische Zeitschrift*, vol. 96, pp. 674–689, 1994.

[31] J. Ackermann, "Robust decoupling, ideal steering dynamics, and yaw stabilization of 4WS cars", *Automatica*, vol. 30, pp. 1761–1768, 1994.

[32] J. Guldner, S. Patwardhan, H.-S. Tan, and W.-B. Zhang, "Coding of road information for automated highways", *ITS Journal*, vol. (submitted), 1996.